

4. SITE 1010¹

Shipboard Scientific Party²

HOLE 1010A

Date occupied: 25 April 1996
Date departed: 25 April 1996
Time on hole: 09 hr, 00 min
Position: 29°57.902'N, 118°6.047'W
Drill pipe measurement from rig floor to seafloor (m): 3475.0
Distance between rig floor and sea level (m): 10.8
Water depth (drill pipe measurement from sea level, m): 3464.2
Total depth (from rig floor, m): 3484.2
Penetration (m): 9.2
Number of cores (including cores having no recovery): 1
Total length of cored section (m): 9.2
Total core recovered (m): 9.2
Core recovery (%): 99.0
Oldest sediment cored:
Depth (mbsf): 9.1
Nature: Silty clay and clayey silt
Age: Quaternary
Comments: A core was taken to establish the mudline.

HOLE 1010B

Date occupied: 25 April 1996
Date departed: 26 April 1996
Time on hole: 04 hr, 30 min
Position: 29°57.905'N, 118°6.044'W
Drill pipe measurement from rig floor to seafloor (m): 3476.3
Distance between rig floor and sea level (m): 10.8
Water depth (drill pipe measurement from sea level, m): 3465.5
Total depth (from rig floor, m): 3499.5
Penetration (m): 23.2
Number of cores (including cores having no recovery): 3
Total length of cored section (m): 23.2
Total core recovered (m): 23.7
Core recovery (%): 102.0
Oldest sediment cored:
Depth (mbsf): 23.71
Nature: Clay
Age: late Pliocene
Measured velocity (km/s): 1.52 at Section 3H-7, 30-33 cm

Comments: Hole terminated because of power failure.

HOLE 1010C

Date occupied: 26 April 1996
Date departed: 27 April 1996
Time on hole: 1 day, 04 hr, 30 min
Position: 29°57.905'N, 118°6.047'W
Drill pipe measurement from rig floor to seafloor (m): 3476.5
Distance between rig floor and sea level (m): 10.8
Water depth (drill pipe measurement from sea level, m): 3465.7
Total depth (from rig floor, m): 3690.4
Penetration (m): 213.9
Number of cores (including cores having no recovery): 24
Total length of cored section (m): 213.9
Total core recovered (m): 192.9
Core recovery (%): 90.0
Oldest sediment cored:
Depth (mbsf): 209.40
Nature: Diatomaceous clay and porcellanite
Age: middle Miocene

Measured velocity (km/s): 1.77 at Section 22X-1, 74-77 cm

Hard rock:

Depth (mbsf): 213.90
Nature: Basalt

Basement:

Depth (mbsf): 209.40
Nature: Basalt

HOLE 1010D

Date occupied: 27 April 1996
Date departed: 27 April 1996
Time on hole: 12 hr, 00 min
Position: 29°57.901'N, 118°6.039'W
Drill pipe measurement from rig floor to seafloor (m): 3477.5
Distance between rig floor and sea level (m): 10.8
Water depth (drill pipe measurement from sea level, m): 3466.7
Total depth (from rig floor, m): 3529.0
Penetration (m): 51.5
Number of cores (including cores having no recovery): 6
Total length of cored section (m): 51.5
Total core recovered (m): 54.5
Core recovery (%): 105.0

¹Lyle, M., Koizumi, I., Richter, C., et al., 1997. *Proc. ODP, Init. Repts.*, 167: College Station, TX (Ocean Drilling Program).

²Shipboard Scientific Party is given in the list preceding the Table of Contents.

Oldest sediment cored:

Depth (mbsf): 51.50
 Nature: Silty clay
 Age: early Pliocene

HOLE 1010E

Date occupied: 27 April 1996

Date departed: 28 April 1996

Time on hole: 1 day, 05 hr, 15 min

Position: 29°57.905'N, 118°6.032'W

Drill pipe measurement from rig floor to seafloor (m): 3476.5

Distance between rig floor and sea level (m): 10.9

Water depth (drill pipe measurement from sea level, m): 3465.6

Total depth (from rig floor, m): 3656.7

Penetration (m): 180.2

Number of cores (including cores having no recovery): 19

Total length of cored section (m): 180.2

Total core recovered (m): 185.2

Core recovery (%): 102.0

Oldest sediment cored:

Depth (mbsf): 180.80
 Nature: Diatom nanofossil ooze, diatom ooze with radiolarians and nanofossils
 Age: middle Miocene

HOLE 1010F

Date occupied: 28 April 1996

Date departed: 29 April 1996

Time on hole: 11 hr, 15 min

Position: 29°57.896'N, 118°6.034'W

Drill pipe measurement from rig floor to seafloor (m): 3476.3

Distance between rig floor and sea level (m): 10.9

Water depth (drill pipe measurement from sea level, m): 3465.4

Total depth (from rig floor, m): 3532.0

Penetration (m): 55.7

Number of cores (including cores having no recovery): 6

Total length of cored section (m): 55.7

Total core recovered (m): 56.8

Core recovery (%): 101.0

Oldest sediment cored:

Depth (mbsf): 55.7
 Nature: Silty clay
 Age: early Pliocene

Comments: Hole was dedicated for interstitial water samples.

Principal results: Site 1010 is the deep-water site (3465 m) of the southern depth transect (Baja Transect) and is situated on 14–15 Ma oceanic crust. The primary objective of drilling at this site was to provide chronological control for biostratigraphic events in the California Current region through the middle Miocene and to investigate the Neogene paleoceanography of the southern region of the California Current. Site 1010 will also be used to study organic matter diagenesis and the ice volume at the last glacial maximum through high-resolution stable isotope profiles of inter-

stitial water. A secondary goal was to obtain a representative sample of the basaltic basement for igneous petrology and geochemistry.

Six holes were cored with the APC/XCB at Site 1010 to a maximum depth of 209.4 mbsf, which recovered an apparently continuous interval of Quaternary to middle middle Miocene sediments (Fig. 1). Hole 1010A is a 9.5-m-long mudline core; Hole 1010B was drilled with the APC to 23.2 mbsf and abandoned because of power failure. Hole 1010C was cored with the APC to 157.5 mbsf and extended with the XCB to 213.9 mbsf. Hole 1010D was cored with the APC to 51.5 mbsf and was terminated because of technical failure. Hole 1010E was cored with the APC to 151.5 mbsf and deepened with the XCB to 180.2 mbsf. Six APC cores were taken at Hole 1010F to 55.7 mbsf. Detailed comparisons between the magnetic susceptibility and GRAPE density record generated on the MST, and high-resolution color reflectance measured with the Oregon State University system, demonstrated complete recovery of the sedimentary sequence down to 110 mbsf.

The sedimentary section begins with approximately 20 m of Quaternary to the uppermost Pliocene siliciclastic sediments with abundant vitric ash layers and disseminated volcanic glass. The underlying unit (38 m thick) contains increased biogenic sediment components with alternating interbeds of nanofossil ooze and silty clay with abundant volcanic ash layers of early to late Pliocene age. This is underlain by ~110 m of clay and nanofossil sediments with increased interbedded siliceous components throughout. The unit ends in the middle middle Miocene and is underlain by a 14–15 Ma basaltic basement, that was cored with the MDCB (Fig. 1). Sedimentation rates throughout the section range from 5–35 m/m.y., averaging 15 m/m.y. Paleomagnetic studies obtained a detailed magnetostratigraphy (Fig. 1) from the Brunhes to the top of Chron C3Bn (7 Ma) and allowed the recognition of the short Cobb Mountain cryptochron.

Biostratigraphic age control was provided by calcareous nanofossils and foraminifers, and siliceous diatoms and radiolarians. The radiolarian assemblages within the Miocene are the best preserved examples of this age from an intense upwelling province and include numerous new species. The planktonic foraminifer assemblages provide a rare insight into the characteristics of faunas associated with intense Miocene upwelling.

The interstitial water geochemistry is typical of an open ocean site, showing the influence of reactions in the underlying basalt via diffusion of the relatively low organic carbon content of the sediments, and of the dissolution of biogenic silica.

BACKGROUND AND OBJECTIVES**General Description**

Site 1010 is the seaward site of the Baja Transect, which crosses the California Current at roughly 30°N. It is located about 100 km north of Guadalupe Island, just seaward of the toe of the Baja California continental slope, on oceanic crust of about 14 Ma in age (Fig. 2). Water depth at Site 1010 is 3480 mbsl. The site was first chosen from a seismic reflection profile from DSDP Leg 63 and surveyed in detail with the *Maurice Ewing* in 1995 (Fig 3). At the drill site, 255 ms of pelagic sediment overlies basement. Layering within the sedimentary section conforms to basement topography and reflects hemipelagic deposition.

Site Objectives

Site 1010 is situated in deep water and has a relatively slow pelagic sedimentation rate (average of about 15 m/m.y. for the total sediment column). Although the site is not suitable for very high-resolution paleoceanographic studies, it was drilled to study the longer term Neogene record. One goal of drilling was to develop a correlation between Neogene biostratigraphic data from the northeastern Pacific and paleomagnetic chronostratigraphy. Because subtropic and subarctic flora and fauna mix along the coast of California, the detailed biostratigraphy fits imperfectly with schema developed for either the

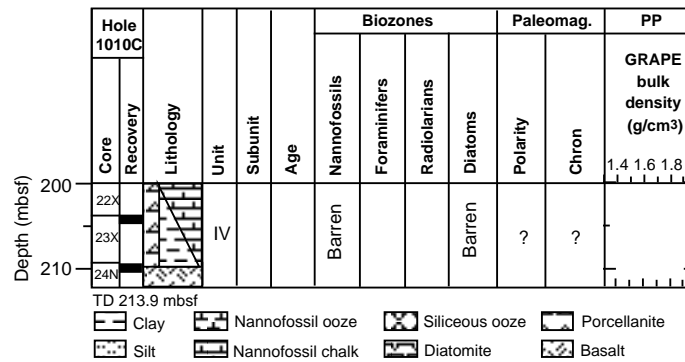


Figure 1 (continued).

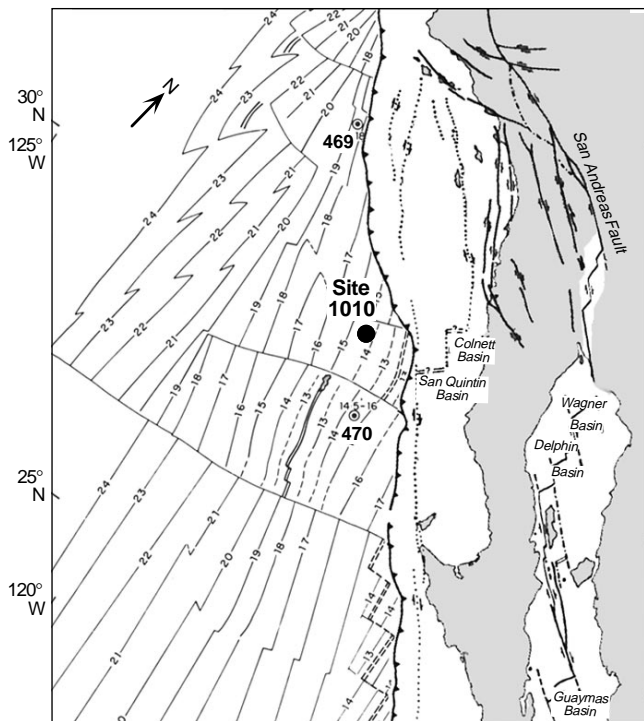


Figure 2. Location map for Site 1010. Crustal ages from Lonsdale (1991). Site 1010 is located about 100 km north of Guadalupe Island on 14–15 Ma oceanic crust. Note: locations of DSDP Sites 469 and 470 are shown for reference.

tropics or the subarctic North Pacific. One important goal of Site 1010 is to provide chronological control for biostratigraphic events in the California Current region through the middle Miocene.

A second important goal is documenting the Neogene paleoceanography of the southern region of the California Current. In the modern oceans, the California Current can be distinguished by its temperature and salinity to the southern tip of Baja California. Site 1010 provides a means to monitor this southern region because it is located underneath the approximate core of the current. The record from this drill site, especially when combined with records from the more northerly transects, will be used to monitor the strength of the California Current flow. Because all the deep-water drill sites on Leg 167 penetrate a large proportion of the Neogene, they will monitor the long-term evolution of the California Current system. Older studies from rotary-cored DSDP drill sites and land sections indicate that sig-

nificant shifts in the strength, or at least the temperature, of the California Current have occurred in the past (Ingle, 1973). Leg 167 drilling will improve our ability to resolve these events. Geochemical indices of paleoproductivity and microfossil assemblages obtained from Site 1010 will also provide important data on nutrients carried by the California Current.

Site 1010 has important geochemical objectives. Organic carbon deposition is relatively high compared to typical pelagic sedimentary sections, yet the sedimentation rate is low. This environment provides one of the end-members needed to study preservation of bulk organic matter and of specific organic molecules. If reliable paleoproductivity indices can be generated, it should also be possible to relate organic matter preservation to flux in low sedimentation-rate environments. We also dedicated a hole at this site for a high-resolution study of interstitial water oxygen and deuterium isotopes. By measuring the interstitial water profile, it is possible to model the isotopic composition of seawater at the last glacial maximum and better constrain the glacial/interglacial shift of isotopic composition. When Cl contents of the interstitial waters are also measured, a second, independent estimate of glacial ice volume can also be made. Because Site 1010 was drilled to oceanic basement, a secondary goal was to obtain a representative sample of the basalt basement for igneous petrology and geochemistry.

OPERATIONS

Acapulco to Site 1010

The 1346-nmi transit from Acapulco to Site 1010 was accomplished in 119 hr at an average speed of 11.3 kt. A 3.5-kHz precision depth recorder (PDR) survey was performed while approaching Site CA-14A, and a Datasonics 354M beacon was dropped on Global Positioning System coordinates at 1045 hr (local time = GMT – 7 hr) on 25 April.

Hole 1010A

Hole 1010A was spudded at 1845 hr on 25 April with an APC/XCB/MDCB coring assembly. A single APC Core 167-1010A-1H was taken from 0 to 9.5 meters below seafloor (mbsf; Table 1; see Table 2 on the CD-ROM in the back pocket of this volume for a more detailed coring summary). A full barrel prevented the establishment of an accurate mudline, and the hole was abandoned.

Hole 1010B

The drill pipe was raised 4 m and Hole 1010B was spudded at 1945 hr on 25 April. The water depth was established at 3475.3 meters below rig floor (mbrf), based on recovery of the mudline core.

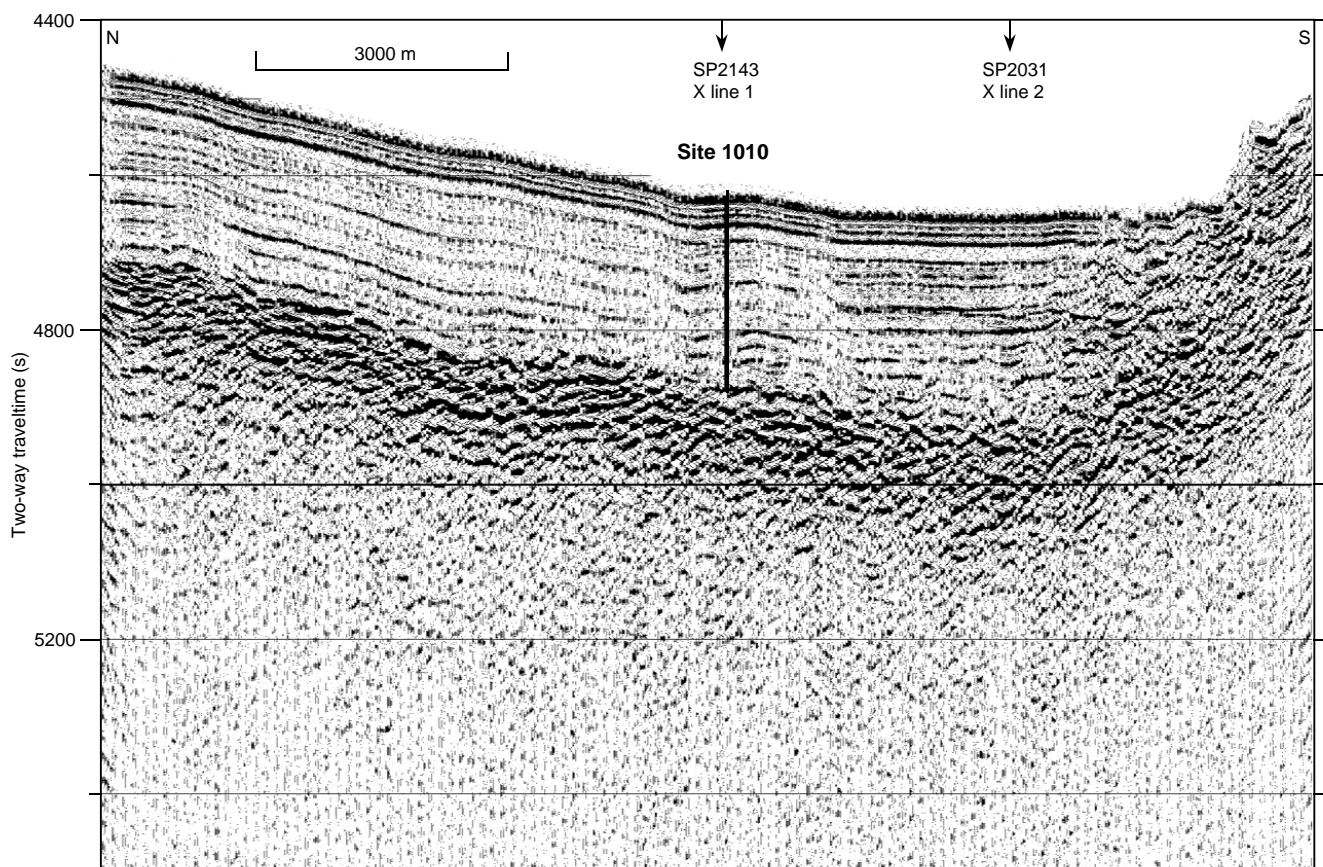


Figure 3. Seismic reflection profile through Site 1010 (Line EW9504 CA14-3; Lyle et al., 1995a, 1995b). Note how sedimentary layering here conforms to basement, indicating hemipelagic sediment deposition. The summed 4-channel data have been filtered between 30 and 200 Hz with predictive deconvolution and Stolt F–K migration applied. On y-axis, (s) = milliseconds.

APC Cores 167-1010B-1H through 3H were taken from 0 to 23.2 mbsf with 102.2% recovery (Table 1). A sudden power failure in the auxiliary 480V transformer temporarily caused a generator to drop off-line. The drill pipe was pulled above the seafloor, ending Hole 1010B, while repairs were made to the generator.

Hole 1010C

The vessel was offset 10 m to the north and Hole 1010C was spudded at 0200 hr on 26 April. The water depth was established at 3476.5 mbrf based on recovery of the mudline core. APC Cores 167-1010C-1H through 17H were taken from 0 to 157.5 mbsf with 103.9% recovery (Table 1). Oriented cores were obtained starting with 3H. XCB Cores 18X through 23X were taken down to 209.4 mbsf with 55% recovery. Excellent recovery was obtained on XCB Cores 18X through 20X, but a chert layer encountered on Core 21X broke off several of the tungsten carbide inserts on the XCB cutting shoe, resulting in a jammed core liner. The inserts were recovered in the core catcher. XCB Cores 22X and 23X were taken with a Carbonado diamond shoe. Core 22X suffered from core jamming and Core 23X encountered basalt and was terminated after 5.6 m advancement in 45 min. One MDCB core was taken down to 213.9 mbsf with a solid section of basalt recovered.

Hole 1010D

Hole 1010D was spudded at 0600 hr on 27 April. The water depth was established at 3477.5 mbrf. APC Cores 167-1010D-1H through

6H were taken from 0 to 51.5 mbsf with 106% recovery (Table 1). Adara heat-flow measurements were performed on Cores 167-1010D-4H through 6H (see “Physical Properties” section, this chapter). Following Core 6H, the coring wireline got wrapped around the sinker bar assembly, trapping the core barrel in the BHA. Attempts to free the core barrel were unsuccessful. We dropped the Kinley cutter and sheared the coring line immediately above the core barrel, which allowed the coring line to be retrieved. The drill string was pulled clear of the seafloor at 1645 hr on 27 April, ending Hole 1010D.

Hole 1010E

After pulling the drill pipe and BHA to the surface, the core barrel was dislodged from the BHA and the pipe was tripped back to bottom. Hole 1010E was spudded at 0430 on 28 April. The water depth was established at 3476.5 mbrf. APC Cores 167-1010E-1H through 16H were taken from 0 to 151.5 mbsf with 103.1% recovery (Table 1). XCB Cores 17X through 19X were taken to 180.2 mbsf with 100.1% recovery. The pipe was pulled clear of the seafloor at 2200 hr on 28 April ending Hole 1010E.

Hole 1010F

The vessel was offset 10 m to the south and Hole 1010F was spudded at 2300 hr on 28 April. The water depth was established at 3476.3 mbrf. APC Cores 167-1010F-1H through 6H were taken down to 55.7 mbsf with 102.3% recovery (Table 1). The drill string was

Table 1. Coring summary for Site 1010.

Core	Date (April 1996)	Time	Top (mbsf)	Bottom (mbsf)	Length cored (m)	Length recovered (m)	Recovery
167-1010A-1H	26	0215	0.0	9.2	9.2	9.15	99.4
167-1010B-1H	26	0315	0.0	4.2	4.2	4.14	98.6
2H	26	0420	4.2	13.7	9.5	9.95	105.0
3H	26	0515	13.7	23.2	9.5	9.62	101.0
167-1010C-1H	26	0915	0.0	5.5	5.5	5.56	101.0
2H	26	1015	5.5	15.0	9.5	9.88	104.0
3H	26	1100	15.0	24.5	9.5	9.82	103.0
4H	26	1200	24.5	34.0	9.5	10.12	106.5
5H	26	1240	34.0	43.5	9.5	10.04	105.7
6H	26	1330	43.5	53.0	9.5	9.97	105.0
7H	26	1410	53.0	62.5	9.5	9.79	103.0
8H	26	1500	62.5	72.0	9.5	9.86	104.0
9H	26	1540	72.0	81.5	9.5	9.87	104.0
10H	26	1630	81.5	91.0	9.5	9.82	103.0
11H	26	1720	91.0	100.5	9.5	9.74	102.0
12H	26	1810	100.5	110.0	9.5	9.82	103.0
13H	26	1900	110.0	119.5	9.5	9.57	101.0
14H	26	2000	119.5	129.0	9.5	9.83	103.0
15H	26	2045	129.0	138.5	9.5	10.07	106.0
16H	26	2140	138.5	148.0	9.5	9.84	103.0
17H	26	2235	148.0	157.5	9.5	9.92	104.4
18X	27	0000	157.5	165.2	7.7	9.44	122.0
19X	27	0100	165.2	174.9	9.7	9.70	100.0
20X	27	0230	174.9	184.6	9.7	6.06	62.5
21X	27	0330	184.6	194.2	9.6	1.18	12.3
22X	27	0630	194.2	203.8	9.6	1.19	12.4
23X	27	0840	203.8	209.4	5.6	0.94	16.8
24N	27	1100	209.4	213.9	4.5	0.91	20.2
167-1010D-1H	27	1315	0.0	4.0	4.0	3.97	99.2
2H	27	1430	4.0	13.5	9.5	10.01	105.3
3H	27	1545	13.5	23.0	9.5	10.12	106.5
4H	27	1700	23.0	32.5	9.5	9.96	105.0
5H	27	1755	32.5	42.0	9.5	10.17	107.0
6H	27	0500	42.0	51.5	9.5	10.24	107.8
167-1010E-1H	28	1200	0.0	9.0	9.0	8.96	99.5
2H	28	1250	9.0	18.5	9.5	9.63	101.0
3H	28	1330	18.5	28.0	9.5	9.99	105.0
4H	28	1415	28.0	37.5	9.5	9.79	103.0
5H	28	1455	37.5	47.0	9.5	9.99	105.0
6H	28	1530	47.0	56.5	9.5	9.95	105.0
7H	28	1630	56.5	66.0	9.5	9.63	101.0
8H	28	1710	66.0	75.5	9.5	9.95	105.0
9H	28	1750	75.5	85.0	9.5	9.65	101.0
10H	28	1830	85.0	94.5	9.5	9.62	101.0
11H	28	1930	94.5	104.0	9.5	10.07	106.0
12H	28	2015	104.0	113.5	9.5	9.65	101.0
13H	28	2110	113.5	123.0	9.5	9.59	101.0
14H	28	2310	123.0	132.5	9.5	9.95	105.0
15H	29	0020	132.5	142.0	9.5	9.86	104.0
16H	29	0115	142.0	151.5	9.5	9.94	104.0
17X	29	0245	151.5	161.0	9.5	9.74	102.0
18X	29	0330	161.0	170.6	9.6	9.62	100.0
19X	29	0415	170.6	180.2	9.6	9.65	100.0
167-1010F-1H	29	0630	0.0	8.2	8.2	8.17	99.6
2H	29	0715	8.2	17.7	9.5	9.58	101.0
3H	29	0800	17.7	27.2	9.5	9.86	104.0
4H	29	0845	27.2	36.7	9.5	9.54	100.0
5H	29	0945	36.7	46.2	9.5	9.88	104.0
6H	29	1030	46.2	55.7	9.5	9.73	102.0

Note: Table 2, on CD-ROM, back pocket, is a more detailed coring summary.

tripped back to the surface and secured for the 8-hr transit to Site 1011 by 0945 hr on 29 April.

LITHOSTRATIGRAPHY

Introduction

A continuous Pleistocene to middle Miocene (0.0 to ~15 Ma) sedimentary sequence was recovered at Site 1010. The sediments vary from siliciclastic to interbedded mixtures of biogenic components (and their diagenetic equivalents) and fine-grained siliciclastics (Fig. 4). Siliciclastic clays and silts are found throughout the cored interval

but predominate in the upper portion. The lower portion consists of sediments containing variable mixtures of biogenic and/or siliciclastic components interbedded on scales 20 to 100 cm. Calcareous nanofossils dominate the calcareous component of the sediments; a mixture of diatoms and radiolarians composes the siliceous fraction. Volcanic glass is abundant and occurs disseminated throughout the dominant lithologies and as distinct ash layers. Volcanic ash content generally decreases with depth; however, discrete vitric ash layers are common throughout the section.

The sediments were divided into four lithostratigraphic units based on visual core descriptions, smear-slide estimates, high-resolution GRAPE bulk density data, and magnetic susceptibility data (Fig.

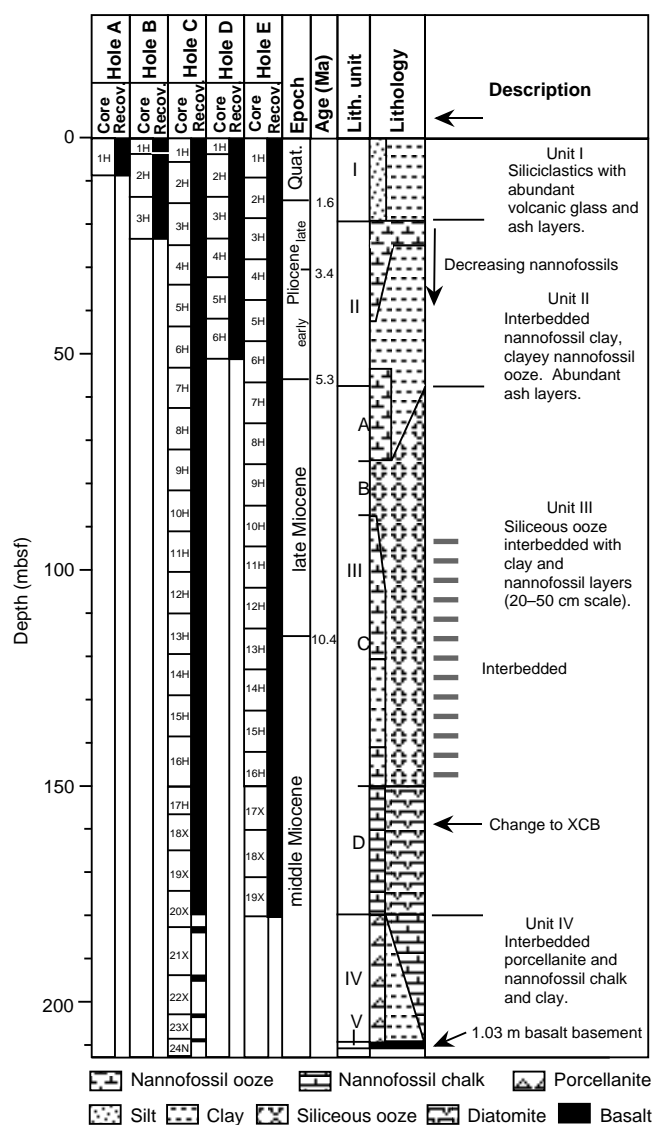


Figure 4. Site 1010 lithostratigraphic summary (0–210.4 mbsf). Hole 1010F split post-cruise; not included in this summary.

4). Unit I is a fine-grained siliciclastic unit composed mainly of clay and silt. Unit II contains calcareous nannofossils interbedded and mixed with siliciclastic material. Unit III consists predominantly of biosiliceous components interbedded and mixed with calcareous nannofossil and clay sediment. Unit IV contains porcellanite interbedded with nannofossil chalk and clay. Basement lithology at this site, designated Unit V, is vesicular aphyric basalt.

Description of Units

Unit I

Hole 1010A, interval 167-1010A-1H, 0–9.15 mbsf (base of core);
 Hole 1010B, interval 167-1010B-1H-1 through 3H-4, 0–18.7 mbsf;
 Hole 1010C, interval 167-1010C-1H-1 through 3H-3, 0–19.0 mbsf;
 Hole 1010D, interval 167-1010D-1H-1 through 3H-5, 0–19.7 mbsf;
 Hole 1010E, interval 167-1010E-1H-1 through 3H-1, 0–19.5 mbsf;
 Hole 1010F, interval 167-1010F-1H-1 through 3H-1, 0–19.0 mbsf.
 Age: Pleistocene to late Pliocene, 0.0–2.6 Ma.

The siliciclastic sediments of Unit I are predominantly clay and silt. Clay content varies from 15% to 80%. The silt component consists mainly of fresh and altered volcanic glass fragments (25%–

40%), quartz (5%–20%), and varying but minor amounts of plagioclase feldspar, biotite, and rock fragments. Calcium carbonate composes less than 5% of the sediment in Unit I. These sediments are dark brown (7.5YR 3/3) to olive gray (5Y 4/2) in color. The color change from brown to green sediments, marking the change from oxidizing conditions above to reducing conditions below (Lyle, 1983), occurs at about 4.2–5.5 mbsf. The dark brown upper portion of this unit contains decimeter-scale dark gray (N3) color bands containing abundant manganese(?) oxide minerals. Several discrete dark gray to black (N4 to N2) vitric ash layers also occur throughout this unit.

Unit II

Hole 1010B, interval 167-1010B-3H-4 through 3H-7, 18.7–23.3 mbsf (base of core);
 Hole 1010C, interval 167-1010C-3H-3 through 7H-2, 19.0–55.1 mbsf;
 Hole 1010D, interval 167-1010D-3H-5 through 6H, 19.7–52.2 mbsf (base of core);
 Hole 1010E, interval 167-1010E-3H-1 through 7H-1, 19.5–56.5 mbsf.
 Hole 1010F, interval 167-1010F-3H-1 through 6H, 19.0–55.7 mbsf (base of core).
 Age: late Pliocene to early Pliocene; 2.6–5.2 Ma.

The upper boundary of Unit II is marked by the first occurrence of abundant biogenic components as indicated by the color change to pale olive (10Y 7/1) and a distinct increase in %CaCO₃ (see “Inorganic Geochemistry” section, this chapter). Unit II consists of an interbedded and variable mixture of calcareous nannofossils and siliciclastic components. Clay content ranges from <10% to >60%, varying inversely with the amount of calcareous material. Coccoliths are the most abundant calcareous component, but foraminifers and discoasters also compose up to 15%. The lithology alternates at a scale of 30–100 cm between olive gray (5Y 5/1) silt- and clay-rich intervals and light olive gray (5Y 7/1) to light greenish gray (5GY 8/1) nannofossil ooze. Bedding contacts are generally gradational and bioturbated. Distinct burrows and hemipelagic laminations are present at a few intervals (Fig. 5). Laminations and thin beds of dark gray (N4) vitric ash and dark green (7.5GY 3/2) altered vitric ash are distributed throughout this unit. The dark gray ash is mostly glass with about 10% finely disseminated opaque minerals. The dark green ash primarily contains glass and clay alteration products.

Unit III

Hole 1010C, interval 167-1010C-7H-2 through 20X-4, 55.1–179.8 mbsf;
 Hole 1010E, interval 167-1010E-7H-1 through 19X-7, 56.5–180.2 mbsf;
 Age: early Pliocene to middle Miocene; 5.2–13.1 Ma.

The transition from Unit II to Unit IIIA occurs with a gradual increase in siliceous components accompanied by a decrease in the GRAPE bulk density of the sediments (see “Physical Properties” section, this chapter). Unit III comprises abundant siliceous microfossil-rich sediments interbedded with calcareous nannofossil and clay-rich intervals. Interbedding throughout this unit is gradational because of pervasive bioturbation. Disseminated volcanic glass is less prevalent in the main lithologies, but distinct vitric ash layers occur abundantly throughout this interval (Fig. 6). The sediments from Unit III are divided into four subunits based on the relative abundance of each component and sediment consolidation character (Fig. 4). Contacts between subunits are not strictly defined because of gradational interbedding of the major lithologies, thus “intervals” given below are only approximate.

Subunit IIIA

Hole 1010C, interval 167-1010C-7H-2 through 9H-4, 55.1–77.7 mbsf;
 Hole 1010E, interval 167-1010E-7H-1 through 9H-2, 56.5–77.5 mbsf.

Subunit IIIA consists of alternating intervals of silty clay containing variable amounts of nannofossils and siliceous microfossils and

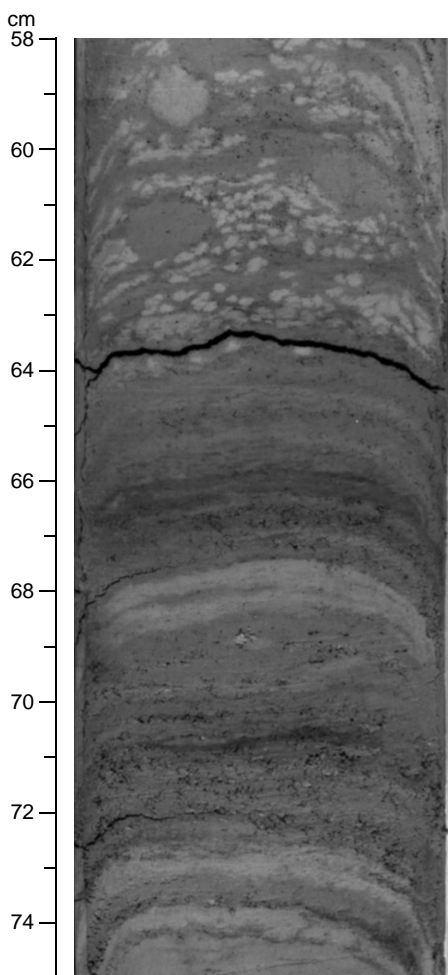


Figure 5. Photograph of distinctly burrowed interval overlying hemipelagic nannofossil-rich laminations in Sample 167-1010D-5H-5, 58–75 cm (Unit II).

nannofossil ooze. Calcium carbonate content in this subunit range from 40% to 70% (see “Inorganic Geochemistry” section, this chapter).

Subunit IIIB

Hole 1010C, interval 167-1010C-7H-4 through 10H-7, 77.5–91.0 mbsf;
Hole 1010E, interval 167-1010E-7H-2 through 10H-5, 77.5–92.5 mbsf.

A gradual transition occurs between Subunit IIIA and Subunit IIIB. GRAPE bulk density decreases slightly as siliceous microfossil content increases at the top of this subunit. Subunit IIIB contains up to 70% diatoms and radiolarians and minor amounts of sponge spicules. Vitric ash is abundant and disseminated throughout this interval.

Subunit IIIC

Hole 1010C, interval 167-1010C-10H-7 through 16H-7, 91.0–148.0 mbsf;
Hole 1010E, interval 167-1010E-10H-5 through 16H-7, 92.5–151.5 mbsf.

A gradual increase in calcareous nannofossil content defines the top of Subunit IIIC. This subunit consists of alternating nannofossil and clay-rich sediments interbedded with the predominant siliceous ooze. Diatoms compose the majority of the siliceous component, although radiolarian and sponge spicules are also common. Intervals of diatom ooze containing 70%–80% diatoms occur at 94.8, 137.9, and 141.0 mbsf.

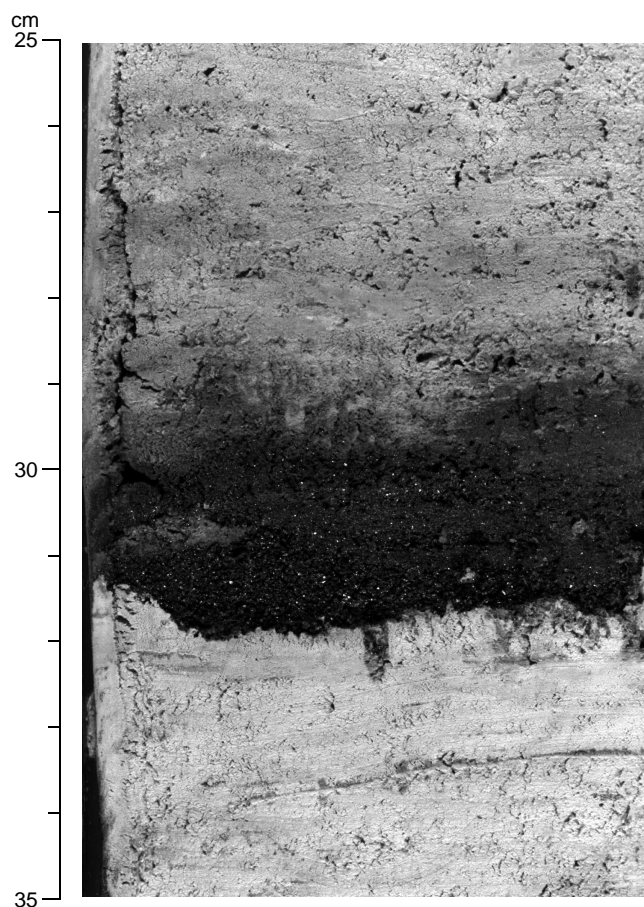


Figure 6. Close-up photograph of vitric ash layer found in Sample 167-1010E-17X-7, 25–35 cm.

Subunit IIID

Hole 1010C, interval 167-1010C-16H-7 through 20X-4, 148.0–179.8 mbsf;
Hole 1010E, interval 167-1010E-16H-7 through 19X-7, 151.5–180.2 mbsf.

Subunit IIID was defined by the transition to more lithified chalks and diatomites marked also by the change from APC to XCB coring. Subunit IIID consists of alternating diatomites and nannofossil chalks with similar sediment composition to Subunit IIIC.

Unit IV

Hole 1010C, interval 167-1010C-20X-4 through 23X, 179.8–209.4 mbsf.
Age: middle Miocene; 13.1–>13.6 Ma.

The top of Unit IV is marked by the first occurrence of porcellanite and consists of interbedded porcellanite, nannofossil chalk, diatomite, and claystone, all containing abundant (5%–35%) disseminated authigenic dolomite. Nannofossil chalk is predominant in the upper part of the interval, but the sediment becomes increasingly clayey and diatomaceous in the lower half of the unit. Nannofossil chalk is completely devoid of diatoms. Very poor recovery (18%) and destruction of softer lithologies prohibited detailed observation of original stratigraphic relationships. Most lithologies in this interval are grayish green (10Y 5/1) to olive gray (5G 5/2) with the exception of minor greenish black (5GY 2/1) chert and silicified clay at the base of the sequence. Porcellanite and chert occur as thin interbeds and concretions, displaying burrows and sedimentary structures similar to those of the surrounding chalk and diatomite. XRD analyses indicate that the diagenetic silica is primarily opal-CT.

Basement Units 1 and 2

Hole 1010C, interval 167-1010C-24N, 209.4–213.9 mbsf.

Basement was reached at 209.4 mbsf and 1.01 m of fine-grained, vesicular aphyric basalt was recovered.

Summary of Lithology

The sedimentary sequence at Site 1010 consists of interbedded siliciclastic clays, nannofossil ooze, and siliceous ooze. These lithologic alternations are also recorded by continuously measured physical properties such as GRAPE density, magnetic susceptibility, and color reflectance data (see “Physical Properties” section, this chapter). Siliceous sediments dominate the Miocene part of the sequence (Units III and IV). This interval is characterized by decimeter-scale (representing a few 100 k.y.) interbedding of siliceous ooze with clay and nannofossil ooze similar to shallower basin deposits of the Monterey Formation of California during this time (Ingle, 1981). A drastic decrease in linear sedimentation rates occurs after about 13–12 Ma (see “Biostratigraphy” section, this chapter), which most likely is related to a reduction in diatom production and burial. Siliceous ooze deposition was reduced further beginning in the late Miocene (5.5 Ma) and was followed by alternating deposition of nannofossil ooze and clay. About 2.5 Ma, sedimentation changed to predominantly siliciclastic clays and silts, and linear sedimentation rates decreased to a few centimeters per thousand years. This change may reflect a decrease in the amount of biogenic deposition and shift to modern processes of hemipelagic deposition at Site 1010 associated with the onset of Northern Hemisphere glaciation.

BIOSTRATIGRAPHY

The sedimentary sequence recovered at Site 1010 consists of an apparently continuous 185-m-thick interval of Quaternary to middle middle Miocene sediments. The section includes an upper 60-m-thick sequence containing variable but often abundant planktonic foraminifers and few diatoms, radiolarians, and calcareous nannofossils from the Quaternary through the earliest Pliocene–latest Miocene. This is underlain by a 70-m-thick sequence of late Miocene to late middle Miocene age marked by an almost complete absence of planktonic foraminifers and generally uncommon calcareous nannofossils, diatoms, and radiolarians. This, in turn, is underlain by a 55-m-thick sequence of rapidly deposited diatom ooze of middle middle Miocene age. These sediments contain abundant diatoms, radiolarians and calcareous nannofossils and few planktonic foraminifers. The base of the sedimentary sequence is assigned to the middle middle Miocene calcareous nannofossil Zone CN4, indicating an age between 13.6 and 15.8 Ma.

Diatoms, radiolarians, and calcareous nannofossils are poorly preserved in the Quaternary through upper middle Miocene sequence and well preserved in the diatom ooze of middle middle Miocene age. They are in sufficient abundance and sufficiently well preserved to provide a well-constrained biostratigraphy and chronology for the entire sequence (Tables 3–9). The few datums that plot off the age/depth curve clearly represent diachronous events (Figs. 7, 8). Assigned ages based on calcareous nannofossils, diatoms, and radiolarians are similar between both Holes 1010C and 1010E. Age/depth plots provide data on changes about sedimentation rates in the sequence. A clear upward reduction in sedimentation rates is shown by all datums in the late middle Miocene at about 12 Ma.

Planktonic foraminifer assemblages exhibit evidence of strong dissolution and fragmentation in most samples of Quaternary through latest Miocene age. Robust and dissolution-resistant species are usually dominant. Quaternary through Pliocene planktonic foraminifer zones are identified but datums are poorly constrained at this time. The absence of planktonic foraminifers from the late Miocene to the late middle Miocene resulted from complete dissolution of assem-

blages. Planktonic foraminifer assemblages of middle middle Miocene age are well preserved and of small size. Zonal marker species are almost completely absent and hence these assemblages are of little biostratigraphic value. Benthic foraminifers are found in most samples in variable abundance and moderately high diversity throughout the sequence, are often dominated by robust, dissolution-resistant species and indicate generally well-oxygenated bottom-water conditions. Middle middle Miocene assemblages often include large species.

The sequence at Site 1010 offers two important opportunities for paleoceanographic and biostratigraphic investigations. The rapidly deposited diatom oozes of middle middle Miocene age contain assemblages of diatoms, radiolarians, and planktonic foraminifers indicative of extensive upwelling of cool waters associated with the California Current. These radiolarian assemblages are the best preserved Miocene examples from an intense upwelling province and include numerous new species never observed before. Likewise, the planktonic foraminifer assemblages provide a rare insight into the characteristics of faunas associated with intense Miocene upwelling. The faunas indicate a severe reduction in upwelling near the beginning of the late Miocene. Diatoms indicate a greater influence of warm waters during parts of the late Miocene.

Changes in planktonic foraminifers of Quaternary through Pliocene age indicate surface-water paleoceanographic changes of large magnitude. Although temperate faunas dominate the sequence, there are large oscillations between tropical and subarctic assemblages. These are associated with the changing strength of the California Current. The sequence of changes in planktonic foraminifers suggests the need to establish a new zonation for the southern California Current system.

The following discussions focus on Holes 1010C and E as few cores were recovered from the other holes. The positions of epoch boundaries are shown in Table 10.

Calcareous Nannofossils

Calcareous nannofossils recovered at Site 1010 were studied from Holes 1010A through 1010E (Table 3). They represent a stratigraphic sequence from the Quaternary (Zone CN13; Okada and Bukry, 1980) through the middle middle Miocene (Zone CN4). Nannofossils are few and generally poorly preserved through the Quaternary. In the Pliocene section, they are common to abundant and the preservation is excellent to moderate. From the upper Miocene to the upper part of the middle Miocene (Zone CN5b) the preservation is poor. Calcareous nannofossils are well preserved and abundant in the middle middle Miocene (Zones CN5a and CN4).

In the Quaternary the nannofossil assemblage is marked by the presence of *Pseudoemiliania lacunosa*, *Calcidiscus leptoporus*, *Helicosphaera carteri*, and several morphotypes of *Gephyrocapsa* spp. and *Ceratolithoides*. The position of the Pleistocene/Pliocene boundary is indicated by the LO (last occurrence) of *Discoaster brouweri*.

Pliocene nannofossil assemblages are marked by several morphotypes of *Reticulofenestra*, *Discoaster*, and *Ceratolithus*. The upper/lower Pliocene boundary, which is close to the LO of *Reticulofenestra pseudoumbilicus* (base of CN12a), occurs between Samples 167-1010C-6H-CC and 7H-CC and between Samples 167-1010E-4H-CC and 5H-CC.

Late Miocene calcareous nannofossils are strongly etched and many marker species are absent or rare. Thus, a precise biostratigraphic assignment of this part in the sequence is difficult. However, the presence of rare *Discoaster quinqueramus/berggrenii* in Samples 167-1010C-9H-3, 6 cm, 1010C-9H-4, 59 cm, and 1010C-8H-CC allows assignment of the upper part of this interval to Zone CN9. A few specimens of *Minylitha convallis* indicate Zones CN8 and CN9a. The presence of rare specimens of *Discoaster hamatus* allows assignment to Zone CN7. In the upper middle Miocene, rare specimens of *Discoaster kugleri* indicate Zone CN5b.

Table 3 (continued).

Zone	Core, section, interval (cm)	Depth (mbsf)	Preservation	Abundance
CN8 (CN9a?)	10H-CC	94.5	M	C
	11H-CC	104	M	F
	12H-CC	113.5	P	F
CN7-CN6?	13H-CC	123	P	F
CN5b?-CN6?	14H-CC	132.5	P	F
CN5b	15H-CC	142	G	A
CN5b?	16H-CC	151.5	G	A
CN5a	17X-CC	161	G	A
CN5a	18X-CC	170.7	G	A
CN5a	19X-CC	180.3	G	A
<i>Pseudoeimiliana lacunosa</i>				
<i>Helicosphaera carteri</i>				
<i>Gephyrocapsa oceanica</i> s.l.				
<i>Gephyrocapsa</i> small				
<i>Gephyrocapsa</i> large				
<i>Discosaster brouweri</i>				
<i>Discosaster</i> <i>triradiatus</i>				
<i>Discosaster pentaradiatus</i>				
<i>Discosaster surculus</i>				
<i>Discosaster tamalis</i>				
<i>Discosaster bellus</i>				
<i>Discosaster bollii</i>				
<i>Sphenolithus</i> spp.				
<i>Reticulofenestra pseudumbilicus</i>				
<i>Reticulofenestra</i> spp.				
<i>Ceratholithus</i> spp.				
<i>Ceratholithus rugosus</i>				
<i>Triquetrorhabdulus rugosus</i>				
<i>Amaurolithus delicatus/tricorniculatus</i>				
<i>Amaurolithus amplifolius</i>				
<i>Amaurolithus</i> spp.				
<i>Discosaster quinquevannus/bergrenii</i>				
<i>Cathaster calyculus</i>				
<i>Discosaster hamatus</i>				
<i>Minyolitha convallis</i>				
<i>Cathaster coalitus</i>				
<i>Coccolithus miopelagicus</i>				
<i>Coccolithus pelagicus</i>				
<i>Discosaster kugleri</i>				
<i>Cyclicargolithus floridanus</i>				
<i>Calcidiscus macintyreii</i> >11 µm				
<i>Calcidiscus macintyreii</i>				
<i>Calcidiscus premacintyreii</i>				
<i>Calcidiscus leporinus</i>				
<i>Sphenolithus heteromorphus</i>				

Note: See "Explanatory Notes" chapter for abbreviations.

The nannofossil assemblage of middle middle Miocene age is dominated by *Cyclicargolithus floridanus* and different morphotypes of *Reticulofenestra*. In Hole 1010C the LO of *Sphenolithus heteromorphus* marks the top of Zone CN4.

Diatoms

Diatoms are common to abundant and moderately well to well preserved throughout the middle Miocene through upper Miocene section. In parts of the Pliocene and Quaternary section, however, diatoms are barren to few (Table 5).

The lower upper Miocene, which is typically marked by both abundant *Denticulopsis hustedtii* and *Denticulopsis dimorpha*, was recovered from Hole 1010E, but not from Hole 1010C (Tables 4, 5). The *Thalassiosira yabei* Zone (NPD 5c) and the *Denticulopsis dimorpha* Zone (NPD 5d) are greatly compressed between Samples 167-1010C-12H-CC and 13H-CC (110.0 through 119.5 mbsf).

Diatom datum levels (Tables 4, 5) indicate continuous and relatively rapid sediment accumulation rates within the Miocene. Although the deep-sea hiatus NH6 of 7.4 to 8.4 Ma age (Keller and Barron, 1987) is widespread in the North Pacific (Barron, 1980), this event was not found because of the poor preservation of diatoms in both Holes 1010C and 1010E.

A special feature of Site 1010 was the recovery of an unusually thick middle Miocene section assignable to the interval of the *Denticulopsis praedimorpha* Zone (NPD 5b) through the underlying *Crucidenticula nicobarica* Zone (NPD 5a).

Correspondingly, the same zones were also observed in the 40-m-thick interval from Samples 167-1010E-14H-CC through 18H-CC. The diatom assemblages of this interval are dominated by *Denticulopsis hustedtii*, *Denticulopsis praedimorpha*, and *Crucidenticula nicobarica*, which are typical middle Miocene species of the subarctic North Pacific Ocean. *Thalassiothrix longissima* and *Thalassionema nitzschioides* are especially abundant in these intervals and are indicative of high oceanic productivity associated with the upwelling conditions.

In Hole 1010E, the lowest Sample 167-1010E-19X-CC contains *Denticulopsis hyalina* and can be correlated with the *D. hyalina* Zone (NPD 4b through 4c).

Radiolarians

Rare and poorly preserved radiolarians were found in the sediments of the upper lithostratigraphic Unit I. Lithostratigraphic Unit II is barren. Abundant and well-preserved radiolarians occurred in the lower lithostratigraphic Unit III. Co-occurrences of dominant mid-latitude species and rare tropical forms differentiate the assemblages of this site from both north Pacific and eastern tropical Pacific radiolarian assemblages (Tables 6, 7).

Presence of *Lamprocyrtis nigrinia* and *L. neoheteroporos* in Sample 167-1010B-2H-CC (13.5 mbsf) is indicative of the Pliocene-Pleistocene. Concurrent occurrence of middle and late Miocene species such as *Anthocyrtidium pliocenica*, *Lychnocanoma n. nipponica*, *Stichocorys peregrina*, *Cyrtocapsella japonica*, and *Diartus hughesi* indicates a highly reworked radiolarian assemblage in Sample 167-1010B-3H-CC (23.2 mbsf).

The interval between Samples 167-1010C-7H-CC and 10H-CC (62.5 to 91 mbsf) is dated as the *S. peregrina* Zone by the presence of common and moderately to well-preserved radiolarians, including marker species such as *Dictyophimus splendens*, *Lamprocyrtis heteroporos*, *S. peregrina*, and *S. delmontensis*. Common and abundant species known to be associated with upwelling regions (*Collosphaera huxleyi*, *Eucyrtidium aderces*, and *Phormostichoartus crustula*) occur within this interval. The continuous occurrence of *D. hughesi* places Samples 167-1010C-11H-CC to 12H-CC (100.5 to 110 mbsf) in the *D. penultima* Zone. Two radiolarian events can be

Table 4. Ranges of diatoms in five holes at Site 1010.

Core, section, interval (cm)	Sample depth (mbsf)	Numeric age (Ma)	Geologic age	Zone	Group abundance	Preservation	Environment	Fragmental diatoms	<i>Actinocyclus ingens</i>	<i>Actinocyclus isugaruensis</i>	<i>Actinoprychus senarius</i>	<i>Arachnoidiscus ehrenbergi</i>	<i>Aulacosira granulata</i>	<i>Azpetitia endoi</i>	<i>Azpetitia nodulifera</i>	<i>Biidulphia aurita</i>	<i>Coscinodiscus lewisianus</i>	<i>Coscinodiscus marginatus</i>
167-1010A-1H-CC	9.2				B													
167-1010B-1H-CC	4.2				B													
2H-CC	13.7	0.3–1.6	Quaternary	NPD 11	T	P/M												
3H-CC	23.2		Pliocene		T	P/M						T						
167-1010C-1H-CC	5.5				B			R										
2H-CC	15.0				B			R										
3H-CC	24.5				B													
4H-CC	34.0				B													
5H-CC	43.5				B													
6H-CC	53.0		Tertiary		R	P		R										
7H-CC	62.5		Tertiary		R	P		F										
8H-CC	72.0				B			R										
9H-CC	81.5		Neogene		F	M												
10H-CC	91.0		Neogene		R	P												
11H-CC	100.5		late Miocene	NPD 6b	A	M/G										T		T
12H-CC	110.0		late Miocene	NPD 6b–NPD 6a	C	P/M							T					D
13H-CC	119.5		late Miocene–middle Miocene	NPD 5c–NPD 5b	A	M/G												C
14H-CC	129.0	9.8–11.4	middle Miocene	NPD 5b	A	M/G	Upwelling	F										
15H-CC	138.5	11.4–12.8	middle Miocene	NPD 5b	D	G	Upwelling								R			
16H-CC	148.0	11.4–12.8	middle Miocene	NPD 5b	D	VG	Upwelling	R										
17H-CC	157.5	11.4–12.8	middle Miocene	NPD 5b	D	VG	Upwelling	R	R									R
18X-CC	165.2	12.8–13.1	middle Miocene	NPD 5a	D	VG	Upwelling	C						R				R
19X-CC	174.9	12.8–13.1	middle Miocene	NPD 5a	D	VG	Upwelling	R									R	
20X-CC	184.6				B													
21X-CC	194.2				B													
23X-CC	209.4				B													
167-1010D-1H-CC	4.0				B													
2H-CC	13.5				B													
3H-CC	23.0				B													
4H-CC	32.5				B													
5H-CC	42.0				B													
6H-CC	51.5	7.1–12.8	late Miocene	NPD 6b–NPD 5b	R	P		R		R								R
167-1010E-1H-CC	9.0				T	P		R										
2H-CC	18.5				B													
3H-CC	28.0				B													
4H-CC	37.5				B													
5H-CC	47.0				B			T										
6H-CC	56.5				R	P		R										
8H-CC	75.5				F	P		C										
9H-CC	85.0	7.1–8.4	late Miocene	NPD 6b	R	P	Upwelling											
10H-CC	94.5	7.1–8.4	late Miocene	NPD 6b	A	G												F
11H-CC	104.0	9.0–9.8	late Miocene	NPD 5d	C	M												A
12H-CC	113.5	9.0–9.8	late Miocene	NPD 5d	C	M												F
13H-CC	123.0	9.8–11.4	late Miocene–middle Miocene	NPD 5c	F	P												F
14H-CC	132.5	11.4–12.8	middle Miocene	NPD 5b	F	P												F
15H-CC	142.0	11.4–12.8	middle Miocene	NPD 5b	A	G	Upwelling											
16H-CC	151.5	11.4–12.8	middle Miocene	NPD 5b	A	G	Upwelling											
17X-CC	161.0	12.8–13.1	middle Miocene	NPD 5b	A	G	Upwelling			R								
18X-CC	170.7	12.8–13.1	middle Miocene	NPD 5a	C	M				R								C
19X-CC	180.3	13.1–14.9	middle Miocene	NPD 5a	A	VG	Upwelling			C								
			middle Miocene	NPD 4c–NPD 4b	F	P												C

Note: See “Explanatory Notes” chapter for abbreviations.

located in this interval: the LO (last occurrence) of the subarctic form *Lychnocanoma n. magnacornuta* (8.8 Ma) between Samples 167-1010C-10H-CC and 11H-CC (91 to 100.5 mbsf), and the LO of *Cyrtocapsella japonica* (10 Ma) between Samples 167-1010C-11H-CC and 12H-CC (100.5 and 110 mbsf). The FO (first occurrence) of *Diartus petterssoni* in Sample 167-1010C-16H-CC (148 mbsf) places the interval between this sample and Sample 167-1010C-13H-CC (120 mbsf) in the middle to late Miocene *D. antepenultima* and *D. petterssoni* Zones. The FO of *L. n. magnacornuta* (12.5 Ma) and the LO of *Lithopera thornburgi* (10.09 Ma) were located within this time interval, between Samples 167-1010C-14H-CC (129 mbsf) and 15H-CC (139 mbsf). The LO of *Eucyrtidium asanoi* between Samples

167-1010C-17H-CC (158 mbsf) and 18H-CC (165 mbsf) appears to be younger (<14.9 Ma) than in the north Pacific (Morley and Nigrini, 1995).

The interval between Samples 167-1010E-8H-CC (75.5 mbsf) and 10H-CC (94.5 mbsf) was placed in the *S. peregrina/D. penultima* Zones because the evolutionary transition between *S. delmontensis* and *S. peregrina* was not clearly observed in moderately preserved assemblages. The LO of *D. hughesi* places the upper limit of the *D. antepenultima/D. petterssoni* Zones in Sample 167-1010E-11H-CC (104 mbsf). The occurrence of a single specimen of *E. asanoi* in Sample 167-1010E-18X-CC (170.7 mbsf) was interpreted as reworking. Radiolarians characteristic of upwelling areas are common in all

Table 4 (continued).

Core, section, interval (cm)	Sample depth (mbsf)	Numeric age (Ma)	Geologic age	Zone	Group abundance	Preservation	Environment	<i>Coscinodiscus marginatus fossilis</i>	<i>Coscinodiscus nodulifer</i>	<i>Coscinodiscus</i> sp.	<i>Crucidentacula nicobarica</i> s.l.	<i>Crucidentacula nicobarica</i> s.s.	<i>Denticulopsis dimorpha</i>	<i>Denticulopsis hustedtii</i>	<i>Denticulopsis hyalina</i>	<i>Denticulopsis lauta</i>	<i>Denticulopsis lauta</i> (miocenica type)	<i>Denticulopsis lauta</i> s.l. in valve view
167-1010A-1H-CC	9.2				B													
167-1010B-1H-CC	4.2				B													
2H-CC	13.7	0.3–1.6	Quaternary	NPD 11	T	P/M			T									
3H-CC	23.2		Pliocene		T	P/M												
167-1010C-1H-CC	5.5				B													
2H-CC	15.0				B													
3H-CC	24.5				B													
4H-CC	34.0				B													
5H-CC	43.5				B													
6H-CC	53.0		Tertiary		R	P						R						T
7H-CC	62.5		Tertiary		R	P						T						T
8H-CC	72.0				B													
9H-CC	81.5		Neogene		F	M												T
10H-CC	91.0		Neogene		R	P												T
11H-CC	100.5		late Miocene	NPD 6b	A	M/G		T										
12H-CC	110.0		late Miocene	NPD 6b–NPD 6a	C	P/M												
13H-CC	119.5	9.8–11.4	late Miocene–middle Miocene	NPD 5c–NPD 5b	A	M/G												
14H-CC	129.0	11.4–12.8	middle Miocene	NPD 5b	A	M/G	Upwelling											
15H-CC	138.5	11.4–12.8	middle Miocene	NPD 5b	D	G	Upwelling	R										
16H-CC	148.0	11.4–12.8	middle Miocene	NPD 5b	D	VG	Upwelling											
17H-CC	157.5	11.4–12.8	middle Miocene	NPD 5b	D	VG	Upwelling											
18X-CC	165.2	12.8–13.1	middle Miocene	NPD 5a	D	VG	Upwelling											
19X-CC	174.9	12.8–13.1	middle Miocene	NPD 5a	D	VG	Upwelling					C						
20X-CC	184.6				B													
21X-CC	194.2				B													
23X-CC	209.4				B													
167-1010D-1H-CC	4.0				B													
2H-CC	13.5				B													
3H-CC	23.0				B													
4H-CC	32.5				B													
5H-CC	42.0				B													
6H-CC	51.5	7.1–12.8	late Miocene	NPD 6b–NPD 5b	R	P												
167-1010E-1H-CC	9.0				T	P												
2H-CC	18.5				B													
3H-CC	28.0				B													
4H-CC	37.5				B													
5H-CC	47.0				R	P												
6H-CC	56.5				F	P												
8H-CC	75.5				R	P												
9H-CC	85.0	7.1–8.4	late Miocene	NPD 6b	A	G	Upwelling											
10H-CC	94.5	7.1–8.4	late Miocene	NPD 6b	C	M												
11H-CC	104.0	9.0–9.8	late Miocene	NPD 5d	C	M												
12H-CC	113.5	9.0–9.8	late Miocene	NPD 5d	F	M												
13H-CC	123.0	9.8–11.4	late Miocene–middle Miocene	NPD 5c	F	P												
14H-CC	132.5	11.4–12.8	middle Miocene	NPD 5b	A	G	Upwelling	R										
15H-CC	142.0	11.4–12.8	middle Miocene	NPD 5b	A	G	Upwelling	R										
16H-CC	151.5	11.4–12.8	middle Miocene	NPD 5b	A	G	Upwelling	R										
17X-CC	161.0	12.8–13.1	middle Miocene	NPD 5a	C	M												
18X-CC	170.7	12.8–13.1	middle Miocene	NPD 5a	A	VG	Upwelling	F		F								
19X-CC	180.3	13.1–14.9	middle Miocene	NPD 4c–NPD 4b	F	P												

samples of the late to middle Miocene. Several new species were observed in these very well-preserved assemblages.

Planktonic Foraminifers

Planktonic foraminifers range from highly abundant to being completely absent in the upper Quaternary through lower Pliocene sequence (from 0 to 63 mbsf) (Tables 8, 9). These changes in abundance reflect strong carbonate dissolution cycles. Assemblages within this interval are moderately to poorly preserved and even the most abundant planktonic foraminiferal assemblages exhibit much evi-

dence of dissolution. Robust species and specimens often dominate, and there is considerable test fragmentation. The dominant forms of the Quaternary and Pliocene are the neogloboquadrinids including *Neogloboquadrina pachyderma* (sinistral and dextral), *Neogloboquadrina asanoi* and *Neogloboquadrina humerosa*, *Globigerina bulloides*, and the globoconellids such as *Globorotalia inflata*. The Quaternary through Pliocene assemblages are predominantly of warm-temperate type, but at times there were incursions of tropical and subarctic elements.

At Site 1010, the base of Quaternary Zone N22/23 is marked by the FO of *Globorotalia truncatulinoides*. The base of late Pliocene

Table 4 (continued).

Core, section, interval (cm)	Sample depth (mbsf)	Numeric age (Ma)	Geologic age	Zone	Group	Abundance	Preservation	Environment	<i>Denticulopsis praedimorpha</i>	<i>Denticulopsis punctata</i>	<i>Denticulopsis simonsenii</i>	<i>Grammatophora</i> sp. (septa)	<i>Neodenticula cf. seminiae</i>	<i>Neodenticula seminiae</i>	<i>Nitzschia</i> sp.	<i>Nitzschia marina</i>	<i>Nitzschia pliocena</i>	<i>Nitzschia porteri</i>	<i>Nitzschia reinholdii</i>		
167-1010A-1H-CC	9.2					B															
167-1010B-1H-CC	4.2	0.3–1.6	Quaternary Pliocene	NPD 11	B																
2H-CC	13.7				T	P/M															
3H-CC	23.2				T	P/M									T	T		T			
167-1010C-1H-CC	5.5					B															
2H-CC	15.0					B															
3H-CC	24.5					B															
4H-CC	34.0					B															
5H-CC	43.5					B															
6H-CC	53.0		Tertiary			R	P														
7H-CC	62.5		Tertiary			R	P														
8H-CC	72.0					B															
9H-CC	81.5		Neogene			F	M														
10H-CC	91.0		Neogene			R	P														
11H-CC	100.5		late Miocene	NPD 6b		A	M/G														
12H-CC	110.0		late Miocene	NPD 6b–NPD 6a		C	P/M														
13H-CC	119.5	9.8–11.4	late Miocene–middle Miocene	NPD 5c–NPD 5b		A	M/G														
14H-CC	129.0	11.4–12.8	middle Miocene	NPD 5b		A	M/G	Upwelling	R												
15H-CC	138.5	11.4–12.8	middle Miocene	NPD 5b		D	G	Upwelling	A												
16H-CC	148.0	11.4–12.8	middle Miocene	NPD 5b		D	VG	Upwelling	D												
17H-CC	157.5	11.4–12.8	middle Miocene	NPD 5b		D	VG	Upwelling	D												
18X-CC	165.2	12.8–13.1	middle Miocene	NPD 5a		D	VG	Upwelling													
19X-CC	174.9	12.8–13.1	middle Miocene	NPD 5a		D	VG	Upwelling													
20X-CC	184.6					B															
21X-CC	194.2					B															
23X-CC	209.4					B															
167-1010D-1H-CC	4.0					B															
2H-CC	13.5					B															
3H-CC	23.0					B															
4H-CC	32.5					B															
5H-CC	42.0					B															
6H-CC	51.5	7.1–12.8	late Miocene	NPD 6b–NPD 5b		R	P		T		R										
167-1010E-1H-CC	9.0					T	P														
2H-CC	18.5					B															
3H-CC	28.0					B															
4H-CC	37.5					B															
5H-CC	47.0					R	P														
6H-CC	56.5					F	P														
8H-CC	75.5					R	P														
9H-CC	85.0	7.1–8.4	late Miocene	NPD 6b		A	G	Upwelling													
10H-CC	94.5	7.1–8.4	late Miocene	NPD 6b		C	M														
11H-CC	104.0	9.0–9.8	late Miocene	NPD 5d		C	M														
12H-CC	113.5	9.0–9.8	late Miocene	NPD 5d		F	M														
13H-CC	123.0	9.8–11.4	late Miocene–middle Miocene	NPD 5c		F	P														
14H-CC	132.5	11.4–12.8	middle Miocene	NPD 5b		A	G	Upwelling	A												
15H-CC	142.0	11.4–12.8	middle Miocene	NPD 5b		A	G	Upwelling	A												
16H-CC	151.5	11.4–12.8	middle Miocene	NPD 5b		A	G	Upwelling	R		R										
17X-CC	161.0	12.8–13.1	middle Miocene	NPD 5a		C	M														
18X-CC	170.7	12.8–13.1	middle Miocene	NPD 5a		A	VG	Upwelling													
19X-CC	180.3	13.1–14.9	middle Miocene	NPD 4c–NPD 4b		F	P														

Zone N21 is marked by the FO of *Globorotalia tosaensis*, the nominate taxa. When the nominate taxa is absent the base of N21 was placed at the FO of *Globorotalia inflata* and *Globorotalia crassaformis*. Early Pliocene Zone N19 in Site 1010 is marked by the presence of *Neogloboquadrina acostaensis* and the absence of typical Pliocene *Globorotalia* species, including *Globorotalia inflata*, *Globorotalia crassaformis*, and *Globorotalia puncticulata*.

The upper Miocene through upper middle Miocene sequence in Site 1010 lacks planktonic foraminifers. However, samples from 56 to 85 mbsf in Hole 1010E contain upper Miocene assemblages consisting of *Globigerina nepenthes*, *Globigerinoides extremus*, *Globigerina woodi*, *Globorotaloides hexagona*, *Sphaeroidinellopsis sem-*

inulina, *Neogloboquadrina acostaensis*, and *Neoglobigerina altispina globosa*.

Below the upper Miocene through upper middle Miocene barren zone, middle middle Miocene diatom-rich sediments contain a small, but well-preserved planktonic foraminiferal assemblage. This assemblage ranges downward to close to basement from 161 mbsf in Hole 1010E and from 148 mbsf in Hole 1010C. These well-preserved faunas are unusual in being dominated by *Globigerina bulloides* and also exhibiting relatively low diversity. Small taxa and individuals are almost completely dominant. An upper middle Miocene age is indicated by an association of *Globorotalia mayeri*, *Globorotaloides variabilis*, *Globorotaloides tremata*, *Orbulina suturalis*, and *Orbulina*

Table 4 (continued).

Core, section, interval (cm)	Sample depth (mbsf)	Numeric age (Ma)	Geologic age	Zone	Group abundance	Preservation	Environment	<i>Paralia sulcata</i>	<i>Rhizosolenia barboi</i>	<i>Rouxia californica</i>	<i>Simonsiella curvirostris</i>	<i>Stephanopyxis turris</i>	<i>Thalassionema cf. schradleri</i>	<i>Thalassionema hiroakienis</i>	<i>Thalassionema nitescioides</i>	<i>Thalassionema nitescioides parva</i>	<i>Thalassionema schradleri</i>					
167-1010A-1H-CC	9.2				B																	
167-1010B-1H-CC	4.2	0.3–1.6	Quaternary Pliocene	NPD 11	B																	
2H-CC	13.7				T	P/M						T							T			
3H-CC	23.2				T	P/M								T						T		
167-1010C-1H-CC	5.5	9.8–11.4 11.4–12.8 11.4–12.8 11.4–12.8 11.4–12.8 12.8–13.1 12.8–13.1	Tertiary Tertiary Neogene Neogene late Miocene late Miocene late Miocene–middle Miocene middle Miocene middle Miocene middle Miocene middle Miocene middle Miocene middle Miocene	NPD 6b NPD 6b–NPD 6a NPD 5c–NPD 5b NPD 5b NPD 5b NPD 5b NPD 5b NPD 5a NPD 5a	B B B B B R R B F A A C A A D D D D D B B B B B R																	
2H-CC	15.0																					
3H-CC	24.5																					
4H-CC	34.0																					
5H-CC	43.5																					
6H-CC	53.0																					T
7H-CC	62.5																					R
8H-CC	72.0																					
9H-CC	81.5																					
10H-CC	91.0																					
11H-CC	100.5																					
12H-CC	110.0																					
13H-CC	119.5																					
14H-CC	129.0																					
15H-CC	138.5																					
16H-CC	148.0																					
17H-CC	157.5																					
18X-CC	165.2																					
19X-CC	174.9																					
20X-CC	184.6																					
21X-CC	194.2																					
23X-CC	209.4																					
167-1010D-1H-CC	4.0	7.1–12.8	late Miocene	NPD 6b–NPD 5b	B B B B B R																	
2H-CC	13.5																					
3H-CC	23.0																					
4H-CC	32.5																					
5H-CC	42.0																					
6H-CC	51.5																					R
167-1010E-1H-CC	9.0	7.1–8.4 7.1–8.4 9.0–9.8 9.0–9.8 9.8–11.4 11.4–12.8 11.4–12.8 11.4–12.8 12.8–13.1 12.8–13.1 13.1–14.9	late Miocene late Miocene late Miocene late Miocene late Miocene–middle Miocene middle Miocene middle Miocene middle Miocene middle Miocene middle Miocene middle Miocene	NPD 6b NPD 6b NPD 5d NPD 5d NPD 5c NPD 5b NPD 5b NPD 5b NPD 5a NPD 5a NPD 4c–NPD 4b	T B B B B R F R A C C F F A A A A C A F																	
2H-CC	18.5																					
3H-CC	28.0																					
4H-CC	37.5																					
5H-CC	47.0																					
6H-CC	56.5																					
8H-CC	75.5																					
9H-CC	85.0																					
10H-CC	94.5																					
11H-CC	104.0																					
12H-CC	113.5																					
13H-CC	123.0																					
14H-CC	132.5																					
15H-CC	142.0																					
16H-CC	151.5																					
17X-CC	161.0																					
18X-CC	170.7																					
19X-CC	180.3																					

universa. This is a cool-water assemblage associated with intensified upwelling and contains few biostratigraphically useful markers.

**PALEOMAGNETISM
Laboratory Procedures**

We made magnetic measurements with the pass-through cryogenic magnetometer on the archive halves of 17 APC cores and one XCB core from Hole 1010C and on 10 APC cores from Hole 1010E. Based

on the results after alternating field (AF) demagnetization, there is a good magnetostratigraphy above 80 mbsf. Some APC cores from 1010E, however, have been affected by drilling disturbance and have an intense magnetic overprint when compared with those from Hole 1010C. In addition to these long sediment sequences, the magnetization before and after AF demagnetization was measured on three and five APC cores from Holes 1010B and 1010D, respectively.

The intensity of natural remanent magnetization (NRM) above 80 mbsf was on the order of 100 mA/m. Below 80 mbsf, the NRM intensity decreases to ~2 mA/m as depth increases. The AF demagnetiza-

Table 4 (continued).

Core, section, interval (cm)	Sample depth (mbsf)	Numeric age (Ma)	Geologic age	Zone	Group abundance	Preservation	Environment	<i>Thalassiosira praeyabei</i>	<i>Thalassiosira</i> sp.	<i>Thalassiosira yabei</i>	<i>Thalassiothrix longissima</i>	<i>Thalassiothrix</i> spp.	Sponge spicules		
167-1010A-1H-CC	9.2				B										
167-1010B-1H-CC	4.2	0.3–1.6	Quaternary Pliocene	NPD 11	B										
2H-CC	13.7				T	P/M			T						
3H-CC	23.2				T	P/M			T						
167-1010C-1H-CC	5.5	9.8–11.4	late Miocene	NPD 6b	B										
2H-CC	15.0				B									F	
3H-CC	24.5				B										
4H-CC	34.0				B										
5H-CC	43.5				B										
6H-CC	53.0					Tertiary		R	P						
7H-CC	62.5					Tertiary		R	P						
8H-CC	72.0							B							
9H-CC	81.5					Neogene		F	M						
10H-CC	91.0					Neogene		R	P					T	
11H-CC	100.5					late Miocene	NPD 6b	A	M/G						
12H-CC	110.0					late Miocene	NPD 6b–NPD 6a	C	P/M						
13H-CC	119.5					late Miocene–middle Miocene	NPD 5c–NPD 5b	A	M/G						
14H-CC	129.0				11.4–12.8	middle Miocene	NPD 5b	A	M/G	Upwelling					
15H-CC	138.5				11.4–12.8	middle Miocene	NPD 5b	D	G	Upwelling					
16H-CC	148.0	11.4–12.8	middle Miocene	NPD 5b	D	VG	Upwelling				A				
17H-CC	157.5	11.4–12.8	middle Miocene	NPD 5b	D	VG	Upwelling	T			C				
18X-CC	165.2	12.8–13.1	middle Miocene	NPD 5a	D	VG	Upwelling				A				
19X-CC	174.9	12.8–13.1	middle Miocene	NPD 5a	D	VG	Upwelling								
20X-CC	184.6				B										
21X-CC	194.2				B										
23X-CC	209.4				B										
167-1010D-1H-CC	4.0	7.1–12.8	late Miocene	NPD 6b–NPD 5b	B										
2H-CC	13.5				B										
3H-CC	23.0				B										
4H-CC	32.5				B										
5H-CC	42.0				B									R	
6H-CC	51.5				R										
167-1010E-1H-CC	9.0	7.1–8.4	late Miocene	NPD 6b	T	P									
2H-CC	18.5				B										
3H-CC	28.0				B										
4H-CC	37.5				B										T
5H-CC	47.0							R	P						R
6H-CC	56.5							F	P						
8H-CC	75.5							R	P						
9H-CC	85.0				7.1–8.4	late Miocene	NPD 6b	A	G	Upwelling					D
10H-CC	94.5				7.1–8.4	late Miocene	NPD 6b	C	M						
11H-CC	104.0				9.0–9.8	late Miocene	NPD 5d	C	M						
12H-CC	113.5				9.0–9.8	late Miocene	NPD 5d	F	M						
13H-CC	123.0				9.8–11.4	late Miocene–middle Miocene	NPD 5c	F	P					F	
14H-CC	132.5				11.4–12.8	middle Miocene	NPD 5b	A	G	Upwelling					D
15H-CC	142.0				11.4–12.8	middle Miocene	NPD 5b	A	G	Upwelling					D
16H-CC	151.5				11.4–12.8	middle Miocene	NPD 5b	A	G	Upwelling					D
17X-CC	161.0	12.8–13.1	middle Miocene	NPD 5a	C	M			R						
18X-CC	170.7	12.8–13.1	middle Miocene	NPD 5a	A	VG	Upwelling								
19X-CC	180.3	13.1–14.9	middle Miocene	NPD 4c–NPD 4b	F	P						D			

tion at 20 mT reduced the remanent magnetization to about 10% of its initial value (Fig. 9). The magnetization of the archive halves had a strong drilling-induced component consisting of a radial (horizontal) and a vertical (z-direction) overprint, as frequently noted on previous legs (e.g., Collot, Greene, Stokking, et al., 1992; Roberts et al., 1996). The radial overprint caused a clustering of declinations around 0°, which became more pronounced with increased depth. We chose an AF of 20 mT to remove as much of the drilling overprint as possible without the risk of inducing an anhysteretic remanent magnetization (ARM) at higher alternating fields. Based on a geocentric axial dipole field, the expected inclination at this site (29°58'N) should be about 49°. Inclinations of the cores from Site 1010 ranged mainly from –60° to +80° for the upper 80 mbsf (Fig. 10) because the pervasive overprint could not be sufficiently removed. We identified normal and reversed polarity chrons in Hole 1010C based on the polarity

of the magnetic inclination. The drilling-induced remanent magnetization (DIRM) in the +z-direction masks the reversal stratigraphy below 80 mbsf (Fig. 9) and makes the identification impossible. The weakened magnetization in the lower intervals corresponds to a lithological change. The sediments above 70 mbsf contain clastic silt or clay, whereas a siliceous component is dominant below (see “Lithostratigraphy” section, this chapter). The stepwise demagnetization of discrete samples in shore-based studies may help to extend the magnetostratigraphy to greater depths.

Results and Discussion

The interpretation of geomagnetic polarity chrons, based on the inclination record at Hole 1010C after 20 mT AF demagnetization, is shown in Figure 10. The reversal boundaries with their depths and as-

Table 6. Ranges of radiolarians in Holes 1010A, 1010B, and 1010C.

Zones	Core, section, interval	Depth (mbsf)	Abundance	Preservation	<i>Actinomma popowski</i>	<i>Amphymenium amphistylium</i>	<i>Anthocyrtidium ehrenbergi</i>	<i>Anthocyrtidium pliocenica</i>	<i>Axopranium angelinum</i>	<i>Axopranium euterpe</i>	<i>Boryostrobos aquilonaris</i>	<i>Boryostrobos bramlettei</i>	<i>Boryostrobos praetumidulus</i>	<i>Boryostrobos tumidulus</i>	<i>Ceratocyrtis histricosus</i>	<i>Collosphaera luxleyi</i>	<i>Cycladophora bicorona</i>	<i>Cycladophora davisiana davisiana</i>	<i>Cyrtocapsella cornuta</i>	<i>Cyrtocapsella japonica</i>	<i>Cyrtocapsella tetrapera</i>	<i>Diartus hughesi</i>	<i>Diartus pettersoni</i>	<i>Dicryophimus splendens</i>	<i>Didymocyrtis prismatica</i>	<i>Eucyrtidium asanoi</i>	<i>Eucyrtidium cabvertense</i>	<i>Eucyrtidium cienkowski</i>	<i>Eucyrtidium cabvertense</i>	<i>Gondwanaria dogeli</i>	<i>Gondwanaria hister</i>	<i>Lamprocyrtis heteroporus</i>	<i>Lamprocyrtis neoheteroporus</i>	<i>Lamprocyrtis nigritiae</i>	<i>Lithopera renzae</i>	<i>Lithopera thornburgi</i>	<i>Lychnocanoma nipponica magnacornuta</i>	<i>Lychnocanoma nipponica nipponica</i>				
Unzoned	167-1010A-1H-CC	9.20	B																																							
Pleistocene	167-1010B-1H-CC 2H-CC 3H-CC	4.20 13.70 23.20	R A C	G G G			R	T		T	F	T		C	R				R	R	F				R				T		T	R							T			
Pleistocene	167-1010C-1H-CC	5.50	R	P															T					T																		
Unzoned	2H-CC 3H-CC 4H-CC 5H-CC 6H-CC	15.00 24.50 34.00 43.50 53.00	B B B R B																																							
Pliocene	7H-CC	62.50	C	G	T		T	F		R	R			T	R								F					T	R													
<i>S. peregrina</i>	8H-CC 9H-CC 10H-CC	72.00 81.50 91.00	B C R	M M	P		P			P	P	P	P	P	P								P	P		P																
<i>D. penultima</i>	11H-CC 12H-CC	100.50 110.00	A A	G G		P	P				P	P									P	P				P															P	
<i>D. ante./D. pet.</i>	13H-CC 14H-CC 15H-CC 16H-CC	119.50 129.00 138.50 148.00	C A A A	M G M G		P	P				P							P	P	P		P	P			P													P	P		
<i>D. alata</i>	17H-CC 18H-CC 19H-CC	157.50 165.20 174.90	A A A	G G G														P		P			P			P			P										P	P		
Unzoned	20X-CC 21X-CC	184.00 194.00	B B																																							

Notes: P = present; more detailed abundance information not available. See "Explanatory Notes" chapter for other abbreviations.

Table 6 (continued).

Zones	Core, section, interval	Depth (mbsf)	Abundance	Preservation	<i>Lychnoedictyum audax</i>	<i>Phormostichoartus corbula</i>	<i>Phormostichoartus crustata</i>	<i>Phormostichoartus doliolum</i>	<i>Phormostichoartus fistula</i>	<i>Prunopyle tetrapila</i>	<i>Siphostichoartus corona</i>	<i>Spirema circularis</i>	<i>Spongodiscus osculosus</i>	<i>Stauraxiphos communis</i>	<i>Stichocorys armata</i>	<i>Stichocorys delmontensis</i>	<i>Stichocorys johnsonii</i>	<i>Stichocorys peregrina</i>	<i>Stichocorys radicata</i>	<i>Stichocorys wolffi</i>	<i>Sylacantarium acquilonium</i>	<i>Sylatractus universus</i>	<i>Sylodictya validispina</i>	<i>Sylosphaera angelina</i>	<i>Theocorys redondoensis</i>	<i>Theocyrtis diabloensis</i>
Unzoned	167-1010A-1H-CC	9.20	B																							
Pleistocene	167-1010B-1H-CC 2H-CC 3H-CC	4.20 13.70 23.20	R A C	G G G	R	R	F F	T	T		T	C	T		C	T	C			C		F			R	
Pleistocene	167-1010C-1H-CC	5.50	R	P									T				T									
Unzoned	2H-CC 3H-CC 4H-CC 5H-CC 6H-CC	15.00 24.50 34.00 43.50 53.00	B B B R B																							
Pliocene	7H-CC	62.50	C	G			T	T		R	F						F			F	T	C				
<i>S. peregrina</i>	8H-CC 9H-CC 10H-CC	72.00 81.50 91.00	B C R	M M		P	P	P	P	P			P		P	P	P	P			P	P	P			
<i>D. penultima</i>	11H-CC 12H-CC	100.50 110.00	A A	G G	P	P		P	P	P			P	P	P		P								P P	
<i>D. ante./D. pet.</i>	13H-CC 14H-CC 15H-CC 16H-CC	119.50 129.00 138.50 148.00	C A A A	M G M G				P		P			P		P	P				P	P	P			P	
<i>D. alata</i>	17H-CC 18H-CC 19H-CC	157.50 165.20 174.90	A A A	G G G				P							P	P									P P P	
Unzoned	20X-CC 21X-CC	184.00 194.00	B B																							

Table 7. Ranges of radiolarians in Holes 1010D and 1010E.

Zones	Core, section, interval	Depth (mbsf)	Abundance	Preservation	<i>Actinomma popowski</i>	<i>Amphymenium amphistylum</i>	<i>Anthocyrtidium ehrenbergi</i>	<i>Anthocyrtidium pliocenica</i>	<i>Axoprunum angelinum</i>	<i>Axoprunum euterge</i>	<i>Botryostrobus aquilonaris</i>	<i>Botryostrobus bramlettei</i>	<i>Botryostrobus praetumidulus</i>	<i>Botryostrobus tumidulus</i>	<i>Ceratocyrtis histricosus</i>	<i>Collosphaera huxleyi</i>	<i>Cycladophora bicorona</i>	<i>Cycladophora davisiana davisiana</i>	<i>Cyrtocapsella cornuta</i>	<i>Cyrtocapsella japonica</i>	<i>Cyrtocapsella tetrapera</i>	<i>Diartus hughesi</i>	<i>Diartus pettersoni</i>	<i>Diccyophimus splendens</i>	<i>Didymocyrtis prismatica</i>	<i>Eucyrtidium asanoi</i>	<i>Eucyrtidium calvertense</i>	<i>Eucyrtidium cienkowskii</i>	<i>Eucyrtidium calvertense</i>	<i>Gondwanaria dogeli</i>	<i>Gondwanaria hister</i>	<i>Lamprocyrtis heteroporos</i>	<i>Lamprocyrtis neoheteroporos</i>	<i>Lamprocyrtis nigritinae</i>			
Unzoned	167-1010D-1H-CC	4.00	R	G																																	
	2H-CC	13.50	R	M													P	P																			
	3H-CC	23.00	B																																		
	4H-CC	32.50	B																																		
	5H-CC	42.00	B																																		
	6H-CC	51.50	B																																		
Unzoned	167-1010E-1H-CC	9.00	B																																		
	2H-CC	18.50	B																																		
	3H-CC	28.00	B																																		
	4H-CC	37.50	B																																		
	5H-CC	47.00	B																																		
	6H-CC	56.50	B																																		
<i>S. peregrina/ D. penultima</i>	8H-CC	75.50	R	M																				T													
	9H-CC	85.00	R	M	P		P						P		P																						
	10H-CC	94.50	C	M		P		P															P														
<i>D. ante./D. pet.</i>	11H-CC	104.00	C	M																																	
	12H-CC	113.50	R	M									P																								
	13H-CC	123.00	C	M																																	
	14H-CC	132.50	A	G																																	
	15H-CC	142.00	C	G																																	
	16H-CC	151.50	A	G																	P																
<i>D. alata</i>	17X-CC	161.00	A	G																																	
	18X-CC	170.70	A	G													P																				
	19X-CC	180.30	A	G													P																				

Notes: P = present; more detailed abundance information not available. See "Explanatory Notes" chapter for other abbreviations.

Table 7 (continued).

Zones	Core, section, interval	Depth (mbsf)	Abundance	Preservation	<i>Lithopora renzae</i>	<i>Lithopora thornburgi</i>	<i>Lychnocanoma nipponica magnicornuta</i>	<i>Lychnocanoma nipponica nipponica</i>	<i>Lychnocricium audax</i>	<i>Phormostichoartus corbula</i>	<i>Phormostichoartus crustula</i>	<i>Phormostichoartus dolioolum</i>	<i>Phormostichoartus fistula</i>	<i>Prunopyle tetrapila</i>	<i>Siphostichoartus corona</i>	<i>Spirema circularis</i>	<i>Spongodiscus osculosus</i>	<i>Stauraxiphos communis</i>	<i>Stichocorys armata</i>	<i>Stichocorys delmontensis</i>	<i>Stichocorys johnsonii</i>	<i>Stichocorys peregrina</i>	<i>Stichocorys radricula</i>	<i>Stichocorys wolffi</i>	<i>Stylacotarium acqulonium</i>	<i>Stylactatus universus</i>	<i>Stylodictya validispina</i>	<i>Stylosphaera angelina</i>	<i>Theocorys redondoensis</i>	<i>Theocorys diabloensis</i>		
Unzoned	167-1010D- 1H-CC 2H-CC 3H-CC 4H-CC 5H-CC 6H-CC	4.00 13.50 23.00 32.50 42.00 51.50	R R B B B B	G M																												
Unzoned	167-1010E- 1H-CC 2H-CC 3H-CC 4H-CC 5H-CC 6H-CC	9.00 18.50 28.00 37.50 47.00 56.50	B B B B B B																													
<i>S. peregrina/ D. penultima</i>	8H-CC 9H-CC 10H-CC	75.50 85.00 94.50	R R C	M M M			P										P			P											T P	
<i>D. ante./D. pet.</i>	11H-CC 12H-CC 13H-CC 14H-CC 15H-CC 16H-CC	104.00 113.50 123.00 132.50 142.00 151.50	C R C A C A	M M M G G G		P			P	P P	P					P				P P P				P							P	
<i>D. alata</i>	17X-CC 18X-CC 19X-CC	161.00 170.70 180.30	A A A	G G G	P P		P P P			P					P P P				P P					P P							P P P P	

Table 10. Position of depth of epoch boundaries according to calcareous nannofossil datum levels.

Boundary	Hole	Depth (mbsf)	Event
Pleistocene/Pliocene	1010C	24.5	T <i>D. brouweri</i>
late/early Pliocene	1010C	72.0	T <i>R. pseudoubilicus</i>
Pliocene/Miocene	1010C	5.8	T <i>D. quinqueramus</i>
late/middle Miocene	1010C	119.5	B <i>D. hamatus</i>

Note: T = top; B = bottom.

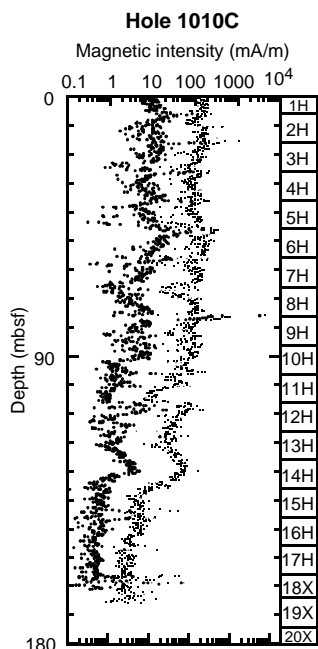


Figure 9. Plot of magnetic intensity of cores from Hole 1010C. Small and large dots represent magnetic intensity before and after AF demagnetization at 20 mT, respectively.

An overview of the shipboard magnetostratigraphy of Site 1010C is given in Figure 10. Results from Hole 1010E are shown in Figure 11.

After correlating the polarity chrons with the standard time scale (Cande and Kent, 1995), an age/depth plot was constructed (Fig. 12). Three linear segments, representing three phases of different sedimentation rate, could be determined in the age/depth plot for the upper 75 mbsf, based on magnetic reversals. During the last 3 m.y., the sedimentation rate ranges around 7 m/m.y. Between 3 and 4 Ma, the sedimentation rate is significantly higher at ~23 m/m.y. In the interval from 7 to 4 Ma, the sedimentation rate is constant at ~11 m/m.y.

COMPOSITE DEPTHS AND SEDIMENTATION RATES

Multisensor track (MST) data collected at 2-cm intervals from Holes 1010A through 1010F and color reflectance data collected at 4-cm intervals from Holes 1010A through 1010E were used to determine depth offsets in the composite section. On the composite depth scale (expressed as mcd, meters composite depth), features of the plotted MST and color reflectance data present in adjacent holes are aligned so that they occur at approximately the same depth. Working from the top of the sedimentary sequence, a constant was added to the

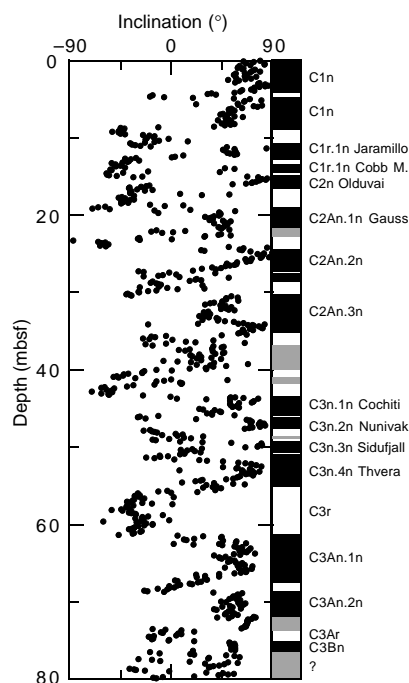


Figure 10. Plot of inclination data from Hole 1010C (after 20 mT AF demagnetization) and correlation with the geomagnetic polarity time scale (Cande and Kent, 1995).

mbsf (meters below seafloor) depth for each core in each hole to arrive at a mcd depth for that core. The depth offsets that compose the composite depth section are given in Table 12 (also on CD-ROM in the back pocket of this volume). Continuity of the sedimentary sequence was documented for the entire sedimentary sequence, although below about 120 mcd, some of the interhole correlations were not of high quality and need to be re-examined in more detail during postcruise processing.

Magnetic susceptibility was primarily used for interhole correlation in the upper 60 mcd, and mainly GRAPE wet-bulk density variations were used below 60 mcd. Color reflectance measurements were used in a few intervals, particularly at the bottom of the section, to provide additional support for composite construction. Natural gamma-ray measurements were made throughout the entire section at all holes, but the sampling interval of 12 cm was insufficient for interhole correlation.

The GRAPE, magnetic susceptibility, and color reflectance records used to verify core overlap for Site 1010 are shown on a composite depth scale in Figures 13, 14, and 15, respectively. The cores from Holes 1010A through 1010F provide continuous overlap to about 60 mcd. Below 60 mcd, the composite record consists only of intervals from Holes 1010C and 1010E. The composite records indicate that 1–3 m of material may be missing between cores in all holes down to about 130 mcd. Below 130 mcd, there appear to be only very small (<10 cm) gaps between holes. This change in the size of gaps between cores in the deeper portion of the sedimentary section may be an artifact because many of the sedimentary features within each core appear to be stretched or compressed.

After constructing the composite depth section for Site 1010, a single spliced record was assembled from the aligned cores. The Site 1010 splice (Table 13, also on CD-ROM, back pocket) can be used as a sampling guide to recover a continuous sedimentary sequence. The spliced record consists entirely of Hole 1010C and 1010E cores.

Table 11. Magnetostratigraphic reversal boundaries in Hole 1010C.

Chronozone boundary	Age (Ma)	Upper limit			Lower limit		
		Core, section	Level (cm)	Depth (mbsf)	Core, section	Level (cm)	Depth (mbsf)
		167-1010C-			167-1010C-		
C1n Brunhes (o)	0.780	2H-3	5	8.55	2H-3	15	8.65
C1r.1n Jaramillo (t)	0.990	2H-4	115	11.15	2H-4	145	11.45
C1r.1n Jaramillo (o)	1.070	2H-5	65	12.15	2H-5	115	12.65
C1r.2r.1n Cobb Mtn. (t)	1.201	2H-6	85	13.85	2H-6	95	13.95
C1r.2r.1n Cobb Mtn. (o)	1.211	2H-6	105	14.05	2H-6	115	14.15
C2n Olduvai (t)	1.770	3H-1	5	15.05	3H-1	15	15.15
C2n Olduvai (o)	1.950	3H-1	105	16.05	3H-1	115	16.15
C2r.2r-1 (t)	2.420	3H-2	65	17.15	3H-2	75	17.25
C2r.2r-1 (o)	2.441	3H-2	95	17.45	3H-2	105	17.55
C2An.1n Gauss (t)	2.581	3H-3	145	19.45	3H-4	35	19.85
C2An.1r Kaena (t)	3.040	3H-5	85	21.85	3H-6	45	22.95
C2An.1r Kaena (o)	3.110	3H-7	5	24.05	3H-7	15	24.15
C2An.2r Mammoth (t)	3.220	4H-2	105	27.05	4H-2	125	27.25
C2An.2r Mammoth (o)	3.330	4H-4	145	30.45	4H-5	5	30.55
C2Ar Gilbert (t)	3.580	5H-2	5	35.55	5H-5	5	40.05
C3n.1n Cochiti (t)	4.180	5H-7	35	43.35	5H-7	55	43.55
C3n.1n Cochiti (o)	4.290	6H-2	85	45.88	6H-2	95	45.98
C3n.2n Nunivak (t)	4.480	6H-2	125	46.28	6H-2	135	46.38
C3n.2n Nunivak (o)	4.620	6H-3	115	47.68	6H-3	125	47.78
C3n.3n Sidufjall (t)	4.800	6H-4	115	49.18	6H-4	135	49.38
C3n.3n Sidufjall (o)	4.890	6H-5	45	49.98	6H-6	5	51.08
C3n.4n Thvera (t)	4.980	6H-6	45	51.48	6H-6	65	51.68
C3n.4n Thvera (o)	5.230	7H-2	105	55.55	7H-3	5	56.05
C3A.n1 (t)	5.894	7H-6	85	61.35	7H-6	95	61.45
C3A.n1 (o)	6.167	8H-4	85	67.85	8H-4	105	68.05
C3A.n2 (t)	6.269	8H-5	25	68.75	8H-5	35	68.85
C3A.n2 (o)	6.567	8H-7	55	72.05	9H-2	5	73.55
C3Bn (t)	6.935	9H-3	5	75.05	9H-3	25	75.25

Notes: o = onset; t = termination; the assigned ages of the reversal boundaries are according to the time scale of Cande and Kent (1995). The upper and lower limits define the range within which a reversal occurs.

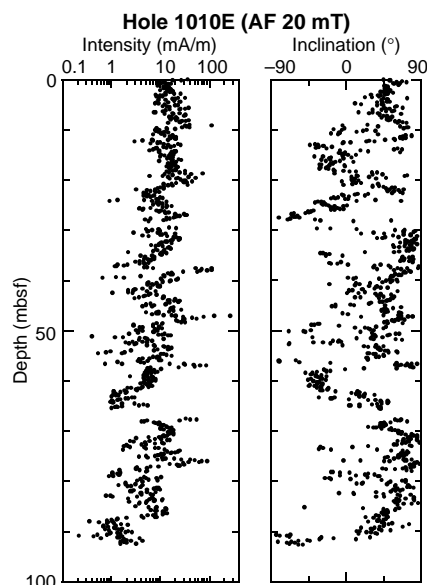


Figure 11. Plots of magnetic intensity and inclination from Hole 1010E (after 20 mT AF demagnetization).

Hole 1010C was used as the backbone of the sampling splice. The composite depths were aligned so that tie points between adjacent holes occurred at exactly the same depths in meters composite depth. Intervals having significant disturbance or distortion were avoided if possible. As mentioned above, several intervals deeper than about 120 mcd did not have an unambiguous overlap between holes.

A preliminary age model (Table 14) was constructed to estimate sedimentation rates (Fig. 16). The age model was applied to the

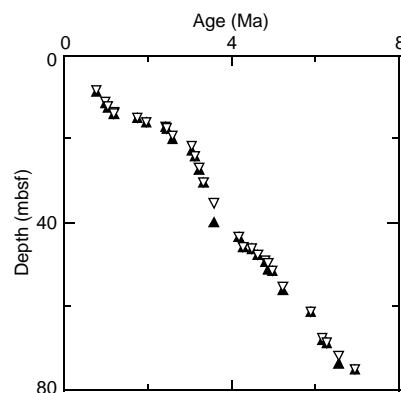


Figure 12. Age/depth plot for Hole 1010C. Open and solid triangles show the upper and lower limits of the magnetostratigraphic reversal boundaries (Cande and Kent, 1995).

spliced records of GRAPE, magnetic susceptibility, and color reflectance shown in Figure 17.

INORGANIC GEOCHEMISTRY

We collected 13 interstitial water samples at Site 1010 for shipboard geochemistry: two from Hole 1010B at depths ranging from 2.95 to 10.15 mbsf and 11 from Hole 1010C at depths ranging from 19.45 to 169.65 mbsf. Primarily for shore-based studies, we collected 35 interstitial water samples, at a frequency of one per section, from Hole 1010F at depths ranging from 1.45 to 55.15 mbsf; a limited suite of shipboard analyses was performed on these samples. For the purpose of this report, samples from different holes are considered to

Table 12. Site 1010 composite depth section.

Core, section	Depth (mbsf)	Offset (m)	Depth (mcd)
167-1010A-1H-1	0.00	0.12	0.12
167-1010B-1H-1	0.00	0.00	0.00
2H-1	4.20	0.38	4.58
3H-1	13.70	2.34	16.04
167-1010C-1H-1	0.00	0.00	0.00
2H-1	5.50	0.86	6.36
3H-1	15.00	2.30	17.30
4H-1	24.50	3.36	27.86
5H-1	34.00	4.86	38.86
6H-1	43.50	5.78	49.28
7H-1	53.00	6.43	59.43
8H-1	62.50	7.49	69.99
9H-1	72.00	7.73	79.73
10H-1	81.50	8.53	90.03
11H-1	91.00	9.43	100.43
12H-1	100.50	10.51	111.01
13H-1	110.00	12.07	122.07
14H-1	119.50	13.05	132.55
15H-1	129.00	13.21	142.21
16H-1	138.50	13.64	152.14
17H-1	148.80	12.76	161.56
18X-1	157.50	13.76	171.26
19X-1	165.20	15.75	180.95
20X-1	174.90	16.33	191.23
167-1010D-1H-1	0.00	0.00	0.00
2H-1	4.00	2.22	6.22
3H-1	13.50	2.98	16.48
4H-1	23.00	5.54	28.54
5H-1	32.50	5.72	38.22
6H-1	42.00	6.59	48.59
167-1010E-1H-1	0.00	0.00	0.00
2H-1	9.00	1.00	10.00
3H-1	18.50	1.50	20.00
4H-1	28.00	4.24	32.24
5H-1	37.50	4.68	42.18
6H-1	47.00	4.95	51.95
7H-1	56.50	6.15	62.65
8H-1	66.00	6.31	72.31
9H-1	75.50	7.39	82.89
10H-1	85.00	8.09	93.09
11H-1	94.50	8.81	103.31
12H-1	104.00	9.53	113.53
13H-1	113.50	11.61	125.11
14H-1	123.00	11.85	134.85
15H-1	132.50	12.35	144.85
16H-1	142.00	11.28	153.28
17X-1	151.50	11.56	163.06
18X-1	161.00	11.70	172.70
19X-1	170.60	14.15	184.75
167-1010F-1H-1	0.00	0.00	0.00
2H-1	8.20	0.78	8.98
3H-1	17.70	2.48	20.18
4H-1	27.20	5.02	32.22
5H-1	36.70	4.72	41.42
6H-1	46.20	5.03	51.23

Note: This table is also on CD-ROM, back pocket, this volume.

constitute a single depth profile. Interstitial water samples are from lithostratigraphic Units I through III (see "Lithostratigraphy" section, this chapter). Chemical gradients in the interstitial waters at this site (Tables 15, 16) reflect the limited amount of organic matter diagenesis, the dissolution of biogenic opal, and the diffusive influence of reactions in the underlying basalt.

Chlorinity increases only slightly downhole by <2% to 569 mM at 76.45 mbsf (Core 167-1010C-9H), then declines to values ~565 mM deeper than 100 mbsf (Fig. 18). Salinity, measured refractively as total dissolved solids, is fairly constant with depth, at 35.0–36.5. Sodium concentrations measured by flame emission spectrophotometry were on average <3% higher than those estimated by charge balance (Table 15).

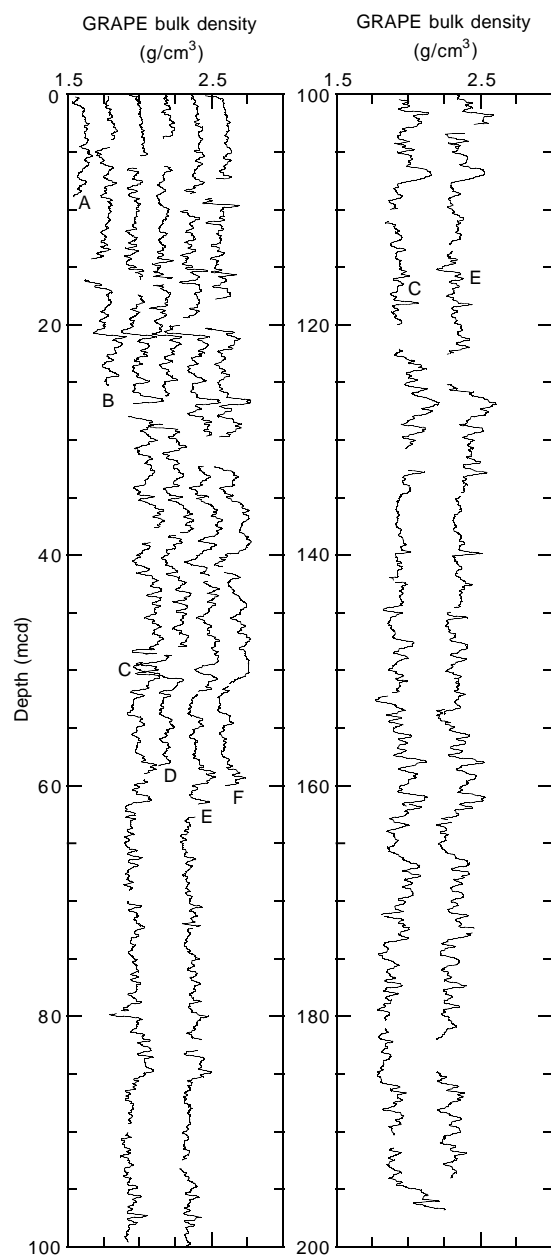


Figure 13. Smoothed GRAPE data from Site 1010 on the mcd scale. Holes 1010A through 1010F are offset from each other by a constant (0.4 g/cm^3).

Alkalinity increases from 3.2 mM at 2.95 mbsf to values >4 mM around 50 mbsf (Fig. 18). Sulfate concentrations are >25 mM throughout the section, indicating the amount of labile organic matter available for oxidation is limited, consistent with the low organic carbon content of these sediments (see "Organic Geochemistry" section, this chapter). Phosphate and ammonium concentrations are relatively low, with phosphate concentrations <10 μM in all samples (nominal detection limit around 1 μM) and ammonium concentrations increasing with depth up to 129 mM at 169.65 mbsf. Phosphate concentrations in the high-resolution interstitial water samples from Hole 1010F document a pronounced maximum in the upper 10 m not revealed by standard sampling intervals (Fig. 18). Dissolved manganese concentrations decrease from 199 μM at 2.95 mbsf to 10 μM at 169.95 mbsf, consistent with suboxic organic carbon diagenesis shallow in the section.

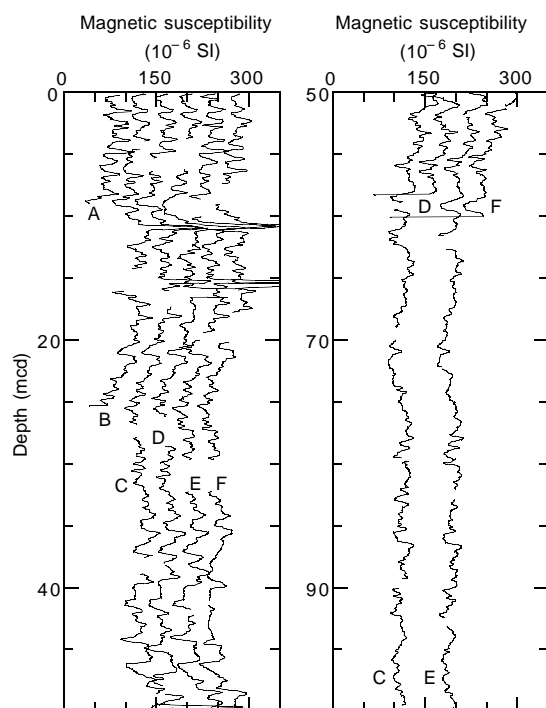


Figure 14. Smoothed (15-point Gaussian) magnetic susceptibility data for the upper 100 m from Site 1010 on the mcd scale. Holes 1010A through 1010F are offset from each other by a constant (40×10^{-6} SI).

Dissolved silicate concentrations increase with depth to values $>1000 \mu\text{M}$ by 80 mbsf (Fig. 18), indicative of the dissolution of biogenic opal. Strontium concentrations increase only slightly with depth.

Calcium concentrations increase with depth, with an average gradient of $4.2 \text{ mM}/100 \text{ m}$ (Fig. 18). Magnesium concentrations decrease with depth, with an average gradient of $-3.3 \text{ mM}/100 \text{ m}$. Mg and Ca concentrations are linearly correlated, with a $\Delta\text{Ca}/\Delta\text{Mg}$ ratio of -1.30 ($R^2 = 0.96$), with the linear correlation and the magnitude of the gradient consistent with the influence of basalt alteration reactions in underlying basement on the observed profiles (McDuff and Gieskes, 1976; McDuff, 1981). Lithium concentrations show only small changes from seawater values (Table 15). Potassium concentrations increase slightly to values $>12 \text{ mM}$ from 30 to 60 mbsf, then decrease to 8.3 mM at 169.65 mbsf.

ORGANIC GEOCHEMISTRY

We conducted measurements of elemental composition and volatile hydrocarbons of sediments from Holes 1010B and 1010C (for methods see "Organic Geochemistry" section, "Explanatory Notes" chapter, this volume).

Volatile Hydrocarbons

Headspace methane concentrations are very low throughout the recovered section (Table 17). This indicates that no significant methanogenesis occurred during diagenesis of organic material, which is consistent with low alkalinity values of the interstitial water samples (see "Inorganic Geochemistry" section, this chapter). Somewhat higher concentrations of methane were present along with ethane, ethene, propane, and propene between 195 and 207 mbsf. These values are probably related to higher temperatures generated during

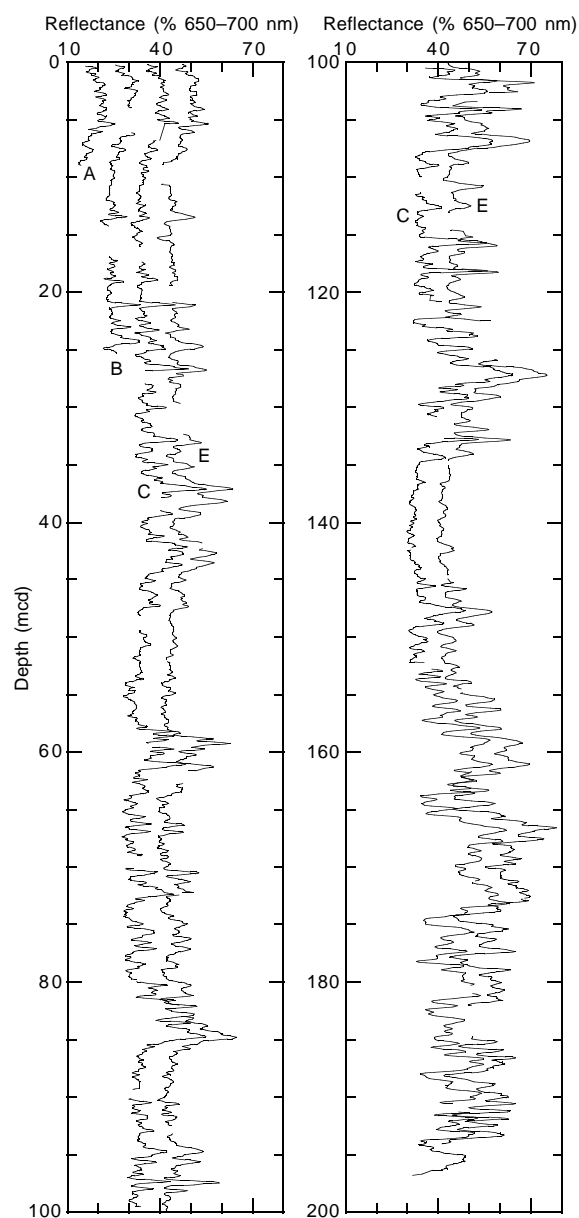


Figure 15. Smoothed (15 point Gaussian) color reflectance (% 650–700 nm band) data from Site 1010 on the mcd scale. Holes 1010A, 1010B, 1010C, and 1010E are offset from each other by a constant (10%).

drilling in the hard formations, however, and are not significant for safety and pollution investigations.

Elemental Analysis

The concentrations of inorganic carbon, total carbon, total nitrogen, and total sulfur are presented in Table 18 (also on CD-ROM, back pocket, this volume) and Figure 19.

The percentage of calcium carbonate (CaCO_3) was calculated from the inorganic carbon concentrations by assuming that all carbonate occurs in the form of calcite. The concentration record of CaCO_3 correlates well with the lithostratigraphic units defined in the "Lithostratigraphy" section, this chapter. In the uppermost 18 mbsf, sediments are characterized by very low carbonate concentrations. The interval between 18 and 120 mbsf shows a high amplitude variation between 0 and 60 wt%. Two distinct intervals of very low

Table 13. Site 1010 splice tie points.

Hole, core, section, interval (cm)	Depth			Hole, core, section, interval (cm)	Depth	
	mbsf	mcd			mbsf	mcd
1010E-1H-5, 95	6.95	6.95	tie to	1010E-1H-1, 0	0.00	0.00
1010C-2H-6, 113	14.13	14.99	tie to	1010C-2H-1, 59	6.09	6.95
1010E-2H-6, 73	17.23	18.23	tie to	1010E-2H-4, 49	13.99	14.99
1010C-3H-6, 35	22.85	25.15	tie to	1010C-3H-1, 93	15.93	18.23
1010E-3H-7, 17	27.67	29.17	tie to	1010E-3H-4, 65	23.65	25.15
1010C-4H-6, 141	33.41	36.77	tie to	1010C-4H-1, 131	25.81	29.17
1010E-4H-6, 125	36.75	40.99	tie to	1010E-4H-4, 3	32.53	36.77
1010C-5H-6, 5	41.55	46.41	tie to	1010C-5H-2, 63	36.13	40.99
1010E-5H-6, 141	46.41	51.09	tie to	1010E-5H-3, 123	41.73	46.41
1010C-6H-4, 5	48.08	53.86	tie to	1010C-6H-2, 28	45.31	51.09
1010E-6H-6, 39	54.89	59.84	tie to	1010E-6H-2, 41	48.91	53.86
1010C-7H-4, 125	58.75	65.18	tie to	1010C-7H-1, 41	53.41	59.84
1010E-7H-6, 45	64.45	70.60	tie to	1010E-7H-2, 103	59.03	65.18
1010C-8H-6, 99	70.99	78.48	tie to	1010C-8H-1, 61	63.11	70.60
1010E-8H-7, 63	75.63	81.94	tie to	1010E-8H-5, 17	72.17	78.48
1010C-9H-6, 87	80.37	88.10	tie to	1010C-9H-2, 71	74.21	81.94
1010E-9H-5, 141	82.91	90.30	tie to	1010E-9H-4, 71	80.71	88.10
1010C-10H-4, 57	86.57	95.10	tie to	1010C-10H-1, 27	81.77	90.30
1010E-10H-7, 25	94.25	102.34	tie to	1010E-10H-2, 51	87.01	95.10
1010C-11H-3, 91	94.91	104.34	tie to	1010C-11H-2, 41	92.91	102.34
1010E-11H-6, 133	103.33	112.14	tie to	1010E-11H-1, 103	95.53	104.34
1010C-12H-5, 47	106.97	117.48	tie to	1010C-12H-1, 113	101.63	112.14
1010E-12H-7, 25	112.83	122.36	tie to	1010E-12H-3, 95	107.95	117.48
1010C-13H-6, 13	117.63	129.70	tie to	1010C-13H-1, 29	110.29	122.36
1010E-13H-6, 79	121.79	133.40	tie to	1010E-13H-4, 9	118.09	129.70
1010C-14H-5, 101	126.51	139.56	tie to	1010C-14H-1, 85	120.40	133.40
1010E-14H-6, 57	131.17	142.92	tie to	1010E-14H-4, 21	127.71	139.56
1010C-15H-6, 121	137.71	150.92	tie to	1010C-15H-1, 71	129.71	142.92
1010E-15H-6, 31	140.31	152.66	tie to	1010E-15H-5, 7	138.57	150.92
1010C-16H-7, 45	147.95	161.59	tie to	1010C-16H-1, 52	139.02	152.66
1010E-16H-6, 141	150.91	162.19	tie to	1010E-16H-6, 81	150.31	161.59
1010C-17H-5, 61	155.41	168.17	tie to	1010C-17H-1, 63	149.43	162.19
1010E-17X-6, 141	160.41	171.97	tie to	1010E-17X-4, 61	156.61	168.17
1010C-18X-4, 113	163.13	176.89	tie to	1010C-18X-1, 71	158.21	171.97
1010E-18X-6, 119	169.69	181.39	tie to	1010E-18X-3, 119	165.19	176.89
1010C-19X-5, 77	171.97	187.72	tie to	1010C-19X-1, 44	165.64	181.39
1010E-19X-5, 143	178.03	192.18	tie to	1010E-19X-2, 147	173.57	187.72
				1010C-20X-1, 95	173.85	192.18

Note: This table is also on CD-ROM, back pocket, this volume.

CaCO₃ contents can be recognized from 42 to 51 mbsf and from 121 to 132 mbsf. These low-carbonate intervals are probably the result of carbonate dissolution, which is suggested by strongly corroded calcareous microfossils (see “Biostratigraphy” section, this chapter). The sediments below 132 mbsf generally contain higher amounts of carbonate, which coincides with abundant well-preserved calcareous nannofossils. Carbonate sedimentation in this interval likely resulted from an enhanced production and preservation of calcareous nannoplankton. In the lowermost part of the sediment column (196 to 205 mbsf), chert-rich sediments show low carbonate values of about 1 to 9 wt%.

Organic carbon concentrations vary generally between 0 and 0.4 wt% throughout the sequence (Table 18; Fig. 19), with some single spikes up to 0.6 wt%. These low concentrations likely reflect (1) little influence of stable terrigenous organic matter and (2) degradation of labile marine organic matter in an oxic depositional environment. A predominantly marine origin of the organic matter is indicated by low TOC/TN ratios ranging between 3 and 5. Because of the very low organic carbon contents, however, TOC/TN ratios have to be used with caution as an indicator of the origin of organic matter. Rock-Eval pyrolysis was not performed because data from these organic carbon-poor sediments would not be reliable.

Sedimentary sulfur contents are extremely low throughout the cores. This indicates that sulfate reduction was inactive during early diagenesis because of an oxic depositional environment.

PHYSICAL PROPERTIES

Multisensor Track Measurements

The shipboard physical properties program at Site 1010 included nondestructive, continuous measurements of bulk density, magnetic

susceptibility, *P*-wave velocity, and natural gamma-ray activity on whole sections of all cores using the MST. GRAPE and PWL measurements were taken at 2-cm intervals for velocity and bulk density, respectively. Magnetic susceptibility was measured at 2-cm intervals at low sensitivity (1-s measuring time), whereas natural gamma-ray activity was measured with a 10-s count every 12 cm (Fig. 20).

Index Properties

Generally, two index properties measurements were made per working section from Holes 1010B and 1010C, and from the first five cores of Hole 1010D. Samples were usually taken from intervals where color reflectivity measurements were made and where samples were collected for calcium carbonate analysis with the objective of determining mass accumulation rates. Index properties (Table 19 on CD-ROM in the back pocket of this volume) were determined using gravimetric method “C” (see “Explanatory Notes” chapter, this volume). After a modified Boyce (1976) correction of -0.1 g/cm^3 is applied, density values measured by GRAPE produce remarkably similar results to those determined by gravimetric methods (Fig. 21). In addition to bulk density, index properties of void ratio, porosity, water content, dry-bulk density, and grain density were determined (Fig. 22).

Compressional-Wave Velocity

P-wave velocity measurements were made, on average, once per working section in Hole 1010B and 1010C (Table 20 on CD-ROM in the back pocket of this volume). The digital sound velocimeter, which measures sonic velocity orthogonal (T2 transducer pair) and parallel (T1 transducer pair) to the core axis (*y*- and *z*-directions, respectively; Fig. 12, “Explanatory Notes” chapter, this volume), was

Table 14. Site 1010 sedimentation rate age control points.

Event	Chron/ subchron	Hole	Depth (mcd)	Age (Ma)
B Brunhes	C1n	1010C	9.46	0.78
T Jaramillo	C1r.1n	1010C	12.16	0.99
B Jaramillo	C1r.1n	1010C	13.26	1.07
T Cobb Mountain	C1r.2r-1n	1010C	14.86	1.20
T Olduvai	C2n	1010C	17.40	1.77
B Olduvai	C2n	1010C	18.40	1.95
T Reunion	C2r.2r-1	1010C	19.50	2.42
B Reunion	C2r.2r-1	1010C	19.80	2.44
T Gauss	C2An.1n	1010C	22.00	2.58
Top	C2An.2n	1010C	26.40	3.11
Bottom	C2An.2n	1010C	30.51	3.22
Top	C2An.3n	1010C	33.86	3.33
T Cochiti	C3n.1n	1010C	48.31	4.18
B Cochiti	C3n.1n	1010C	51.71	4.29
T Nunivak	C3n.2n	1010C	52.11	4.48
B Nunivak	C3n.2n	1010C	53.51	4.62
T Sidufjall	C3n.3n	1010C	55.06	4.80
T Thvera	C3n.4n	1010C	57.36	4.98
B Thvera	C3n.4n	1010C	62.23	5.23
Top	C3An.1n	1010C	67.83	5.89
Bottom	C3An.1n	1010C	75.28	6.14
Top	C3An.2n	1010C	76.13	6.27
Top	C3Bn	1010C	82.88	6.94
<i>T D. hamatus</i>		1010C	109.93	9.49
<i>B D. hamatus</i>		1010C	137.30	10.50
<i>T D. kugleri</i>		1010E	139.60	11.44
<i>T C. premacintyrei</i>		1010E	167.45	12.22
<i>FCO D. hustedtii</i>		1010C	185.80	13.10
<i>T S. heteromorphus</i>		1010C	203.65	13.60

Note: T = top, B = bottom, FCO = first common occurrence.

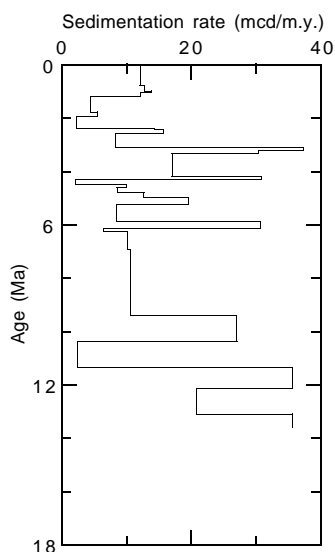


Figure 16. Sedimentation rate vs. age based on the age control points from Table 14.

used to a depth of 9 mbsf in Hole 1010B. The sediment is too consolidated below this depth to use the insertable transducers, and the Hamilton Frame velocimeter (T3) was used for the remainder of the hole and for all of Hole 1010C. This device measures velocity in the x-direction and was used through the liner. *P*-wave velocity values range from 1480 to 1630 m/s with an average of 1502 m/s in Hole 1010B and from 1420 to 1590 m/s with an average of 1522 m/s in Hole 1010C (Table 20 on CD-ROM in the back pocket of this volume), reflecting a gradual downhole increase in velocity in Hole 1010C of approximately 0.24 m/s per 1 m (Fig. 23). Below 117.5 mbsf in Hole 1010C, the sediments are fractured and the PWL was not used.

Heat Flow

Thermal conductivity was measured in the sediment cores of Holes 1010D and 1010E (Table 21 on CD-ROM in the back pocket of this volume) approximately every 2 m to 64.75 mbsf. The APC temperature tool yielded no useful result at 24.5 mbsf (Core 167-1010D-3H) because the extremely soft nature of the sediment allowed too much movement of the tool, causing frictional heat disturbances (Fig. 24). However, three good-quality measurements were collected: 5.4°C at 34.0 mbsf, 6.5°C at 43.5 mbsf, and 8.2°C at 53.0 mbsf (Cores 167-1010D-4H, 5H, and 6H, respectively). In addition to these three data points, the bottom-water temperature for Core 167-1010D-5H was measured during the run. The tool was left about 20 m above the seafloor for approximately 3.5 min before and after piston coring, yielding a bottom-water temperature of 1.5°C ± 0.1°C. The four data points give a thermal gradient of 122°C/km (Fig. 25). Using an average measured thermal conductivity of 0.962 W/(m·K) provides a heat-flow estimate of 118 mW/m² at Site 1010.

Color Reflectance

Color reflectance was measured at intervals of 4 to 6 cm at Site 1010. Data from the upper 50 m of Hole 1010E are summarized in Figure 26A for averages of two 50-nm-wide bandwidths: 450–500 nm (blue) and 650–700 nm (red). The composite reflectance section to 180 mbsf for the 650–700-nm band average is included in the “Composite Depths and Sedimentation Rates” section (this chapter). Percent reflectance in the visible wavelengths averages about 20%, but the signal displays high-amplitude, cyclical variability, especially below 20 mbsf. These fluctuations are similar to the shipboard calcium carbonate data, both in amplitude and phase (“Organic Geochemistry” section, this chapter). Each sediment type at Site 1010 has a unique reflectance spectrum (Fig. 26B–E). For example, the uppermost 6 m of Hole 1010E is predominantly yellowish brown silty clay (Fig. 26B) and displayed a spectrum distinct from the brown/green silty clay (Fig. 26C). Both clays exhibited low reflectance (10%–20%), but the former reflected more strongly in the red to infrared portion of the spectrum. The ubiquitous ash layers at this site exhibited low reflectance (<10%) and a uniquely flat spectrum from 250 to 950 nm (Fig. 26D). In stark contrast, nanofossil ooze yielded reflectance values near 40%, with strong reflectance in the middle of the visible range and a reflectance minimum near 700 nm (Fig. 26E). The shape of this spectrum is similar to that reported for nanofossil ooze at ODP Leg 138 sites in the eastern equatorial Pacific (Mayer, Pisias, Janecek, et al., 1992).

Digital Color Video

Images from the ODP color digital imaging system were captured from all cores from Site 1010. The images were taken over 20-cm intervals, providing a 0.25-mm pixel. At Hole 1010D a good correlation exists between the intensity of color CIELAB L* (see “Explanatory Notes” chapter, this volume) and GRAPE bulk density (Fig. 27), most likely reflecting variance in calcium carbonate content.

SUMMARY

Site 1010 is the seaward site of the Baja Transect, drilled on middle Miocene ocean crust in 3476 m water depth. We achieved our objective to drill the entire 210-m-thick sedimentary column to basaltic basement (Fig. 28). The oldest sediments at Site 1010 were laid down at ~14 Ma and are the oldest sediments recovered during Leg 167. The sediment column was double-cored to 180 mbsf (~13 Ma), and triple-cored to 51 mbsf (~4.3 Ma). Magnetic stratigraphy is of high quality at this site through the top of Chronozone C3Bn (6.94 Ma), and the stratigraphy may be extended further by shore-based studies.

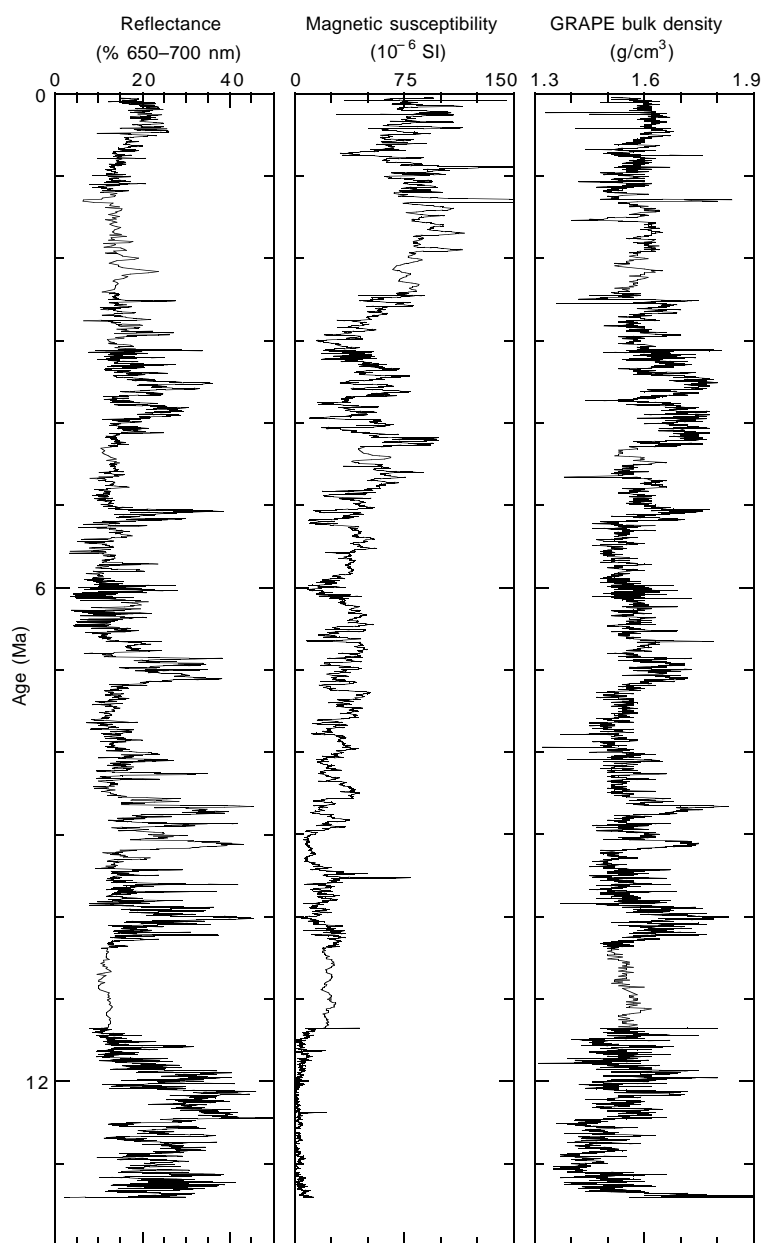


Figure 17. Spliced records of color reflectance, magnetic susceptibility, and GRAPE bulk density vs. age based on age control points from Table 14.

Distinctive features to note about the sediment column are the relatively high accumulation rates of opal-rich sediments during the Miocene, shifting abruptly at the Miocene/Pliocene boundary to clays with variable calcium carbonate content. An interval of high calcium carbonate content occurs in upper Pliocene sediments, followed by a microfossil-poor Pleistocene section. Highest calcium carbonate MARs occur between 3 and 4 Ma and before 12 Ma. Site 1010 was the location of a high-resolution interstitial water sampling program designed to better define the oxygen isotope excursion associated with the last glacial maximum.

REFERENCES

- Barron, J.A., 1980. Lower Miocene to Quaternary diatom biostratigraphy of Leg 57, off Northeastern Japan, Deep Sea Drilling Project. In von Huene, R., Nasu, N., et al., *Init. Repts. DSDP*, 56, 57 (Pt. 2): Washington (U.S. Govt. Printing Office), 641–685.
- Boyce, R.E., 1976. Definitions and laboratory techniques of compressional sound velocity parameters and wet-water content, wet-bulk density, and porosity parameters by gravimetric and gamma-ray attenuation techniques. In Schlanger, S.O., Jackson, E.D., et al., *Init. Repts. DSDP*, 33: Washington (U.S. Govt. Printing Office), 931–958.
- Cande, S.C., and Kent, D.V., 1995. Revised calibration of the geomagnetic polarity timescale for the Late Cretaceous and Cenozoic. *J. Geophys. Res.*, 100:6093–6095.
- Collot, J.-Y., Greene, H.G., Stokking, L.B., et al., 1992. *Proc. ODP, Init. Repts.*, 134: College Station, TX (Ocean Drilling Program).
- Ingle, J.C., Jr., 1973. Summary comments on Neogene biostratigraphy, physical stratigraphy, and paleo-oceanography in the marginal northeastern Pacific Ocean. In Kulm, L.D., von Huene, R., et al., *Init. Repts. DSDP*, 18: Washington (U.S. Govt. Printing Office), 949–960.
- Ingle, J.C., Jr., 1981. Origin of Neogene diatomites around the north Pacific rim. In Garrison, R.E., Douglas, R., Pisciotto, K., Isaacs, C., and Ingle, J.C. (Eds.), *The Monterey Formation and Related Siliceous Rocks of California*. Spec. Publ.—Soc. Econ. Paleontol. Mineral., 15:159–179.
- Keller, G., and Barron, J.A., 1987. Paleodepth distribution of Neogene deep-sea hiatuses. *Paleoceanography*, 2:697–713.
- Lonsdale, P., 1991. Structural patterns of the Pacific floor offshore of Peninsular California. In Dauphin, J.P., and Simoneit, B.R.T. (Eds.), *The Gulf and Peninsular Province of the Californias. Amer. Assoc. Petrol. Geol. Memoir* 47, 87–125.

- Lyle, M., 1983. The brown-green transition in marine sediments: a marker of the Fe(III)–Fe(II) redox boundary. *Limnol. Oceanogr.*, 28: 1026–1033.
- Lyle, M., Gallaway, P.J., Liberty, L.M., Mix, A., Stott, L., Hammond, D., Gardner, J., Dean, W., and the EW9504 Scientific Party, 1995a. Data submission. W9406 and EW9504 site surveys of the California margin proposed drillsites, Leg 167. Volume 1: Site maps and descriptions. *Boise State University, CGISS Tech. Rept.*, 95–11.
- Lyle, M., Gallaway, P.J., Liberty, L.M., Mix, A., Stott, L., Hammond, D., Gardner, J., Dean, W., and the EW9504 Scientific Party, 1995b. Data submission. W9406 and EW9504 site surveys of the California margin proposed drillsites, Leg 167. Volume 2: Seismic profiles. *Boise State University, CGISS Tech. Rept.*, 95–12.
- Mayer, L., Pisias, N., Janecek, T., et al., 1992. *Proc. ODP, Init. Repts.*, 138 (Pts. 1 and 2): College Station, TX (Ocean Drilling Program).
- McDuff, R.E., 1981. Major cation gradients in DSDP interstitial waters: the role of diffusive exchange between seawater and upper oceanic crust. *Geochim. Cosmochim. Acta*, 45:1705–1713.
- McDuff, R.E., and Gieskes, J.M., 1976. Calcium and magnesium profiles in DSDP interstitial waters: diffusion or reaction? *Earth Planet. Sci. Lett.*, 33:1–10.
- Morley, J.J., and Nigrini, C., 1995. Miocene to Pleistocene radiolarian biostratigraphy of North Pacific Sites 881, 884, 885, 886, and 887. *In* Rea, D.K., Basov, I.A., Scholl, D.W., and Allan, J.F. (Eds.), *Proc. ODP, Sci. Results*, 145: College Station, TX (Ocean Drilling Program), 55–91.
- Okada, H., and Bukry, D., 1980. Supplementary modification and introduction of code numbers to the low-latitude coccolith biostratigraphic zonation (Bukry, 1973; 1975). *Mar. Micropaleontol.*, 5:321–325.
- Roberts, A.P., Stoner, J.S., and Richter, C., 1996. Coring induced magnetic overprints and limitations of the long-core paleomagnetic measurements technique: some observations from Leg 160, eastern Mediterranean Sea. *In* Emeis, K.-C., Robertson, A.H.F., Richter, C., et al., *Proc. ODP, Init. Repts.*, 160: College Station, TX (Ocean Drilling Program), 497–505.

Ms 167IR-104

NOTE: For all sites drilled, core-description forms (“barrel sheets”) and core photographs can be found in Section 3, beginning on page 499. Smear-slide data can be found in Section 4, beginning on page 1327. Thin section data can be found in Section 5, beginning on page 1375. See Table of Contents for material contained on CD-ROM.

Table 15. Interstitial water geochemical data, Holes 1010B and 1010C.

Core, depth, interval (cm)	Depth (mbsf)	pH	Alkalinity (mM)	Salinity	Cl ⁻ (mM)	Na ⁺ (mM)	SO ₄ ²⁻ (mM)	HPO ₄ ²⁻ (μM)	NH ₄ ⁺ (μM)	H ₄ SiO ₄ (μM)	Mn ²⁺ (μM)	Ca ²⁺ (mM)	Mg ²⁺ (mM)	Sr ²⁺ (μM)	Li ⁺ (μM)	K ⁺ (mM)
167-1010B-																
1H-2, 145–150	2.95	7.59	3.16	35.5	559	481	28.6	6.1	16	374	199	10.7	52.8	79	28	11.5
2H-4, 145–150	10.15	7.73	3.69	35.0	559	482	28.8	6.2	27	490	133	10.8	52.4	75	25	11.8
167-1010C-																
3H-3, 145–150	19.45	7.57	4.10	35.0	558	480	28.0	2.3	64	516	97	11.4	51.9	75	29	11.8
4H-3, 145–150	28.95	7.40	3.86	35.0	562	480	26.8	2.1	82	553	88	11.9	52.1	79	29	11.9
5H-3, 145–150	38.45	7.41	3.83	36.0	562	481	27.6	3.2	85	809	80	12.2	51.2	79	30	13.1
6H-3, 145–150	47.98	7.83	4.44	35.5	564	485	28.2	2.6	97	707	69	13.2	50.8	81	31	12.2
7H-3, 145–150	57.45	7.53	4.01	36.0	566	486	28.5	2.5	102	910	71	13.3	50.5	82	31	13.0
8H-3, 145–150	66.95	7.78	3.69	36.5	568	490	28.3	2.7	112	892	56	13.2	50.1	82	31	11.3
9H-3, 145–150	76.45	7.39	3.51	35.0	569	485	26.8	2.1	114	1043	64	13.2	50.3	81	31	13.7
10H-3, 145–150	85.95	7.40	3.42	36.5	568	488	27.4	2.4	120	1110	46	13.8	50.0	87	31	10.5
13H-3, 145–150	114.45	7.37	3.64	35.0	566	481	24.6	2.5	122	1209	29	14.8	49.4	85	31	9.9
16H-3, 145–150	142.95	7.40	3.82	35.0	561	477	25.7	2.9	124	1321	14	16.5	48.8	92	29	9.0
19X-3, 145–150	169.65	7.34	3.91	35.0	565	484	26.7	2.5	129	1332	10	17.7	47.2	93	27	8.3

Table 16. Interstitial water geochemical data, Hole 1010F.

Core, section, interval (cm)	Depth (mbsf)	pH	Alkalinity (mM)	Salinity	HPO ₄ ²⁻ (μM)
167-1010F-					
1H-1, 145–150	1.45	7.61	3.11	35	5.2
1H-2, 145–150	2.95			38	9.2
1H-3, 145–150	4.45			35	8.4
1H-4, 145–150	5.95	7.56	3.36	35	9.5
1H-5, 145–150	7.45			35	8.5
2H-1, 145–150	9.65	7.90	3.73	35	7.5
2H-2, 145–150	11.15			35	5.2
2H-3, 145–150	12.65			35	4.5
2H-4, 145–150	14.15	7.74	3.57	35	3.8
2H-5, 145–150	15.65				3.9
2H-6, 135–140	17.05				3.3
3H-1, 145–150	19.15	7.99	3.02	35	2.9
3H-2, 145–150	20.65				2.8
3H-3, 145–150	22.15				2.5
3H-4, 145–150	23.65	7.02	3.30	35	3.7
3H-5, 145–150	25.15				3.4
3H-6, 145–150	26.65				4.0
4H-1, 145–150	28.65	7.72	3.30	35	3.1
4H-2, 145–150	30.15				2.2
4H-3, 145–150	31.65				1.8
4H-4, 145–150	33.15	7.04	2.05	35	1.5
4H-5, 145–150	34.65				1.4
4H-6, 135–140	36.05				1.9
5H-1, 145–150	38.15	7.37	3.34	35	1.9
5H-2, 145–150	39.65				1.7
5H-3, 145–150	41.15				2.0
5H-4, 145–150	42.65	7.65	3.53	35	1.7
5H-5, 145–150	44.15				2.6
5H-6, 145–150	45.65				2.0
6H-1, 145–150	47.65	8.10	4.26	35	1.7
6H-2, 145–150	49.15				2.0
6H-3, 145–150	50.65				1.9
6H-4, 145–150	52.15	8.02	3.71	35.5	1.6
6H-5, 145–150	53.65				1.5
6H-6, 145–150	55.15				1.3

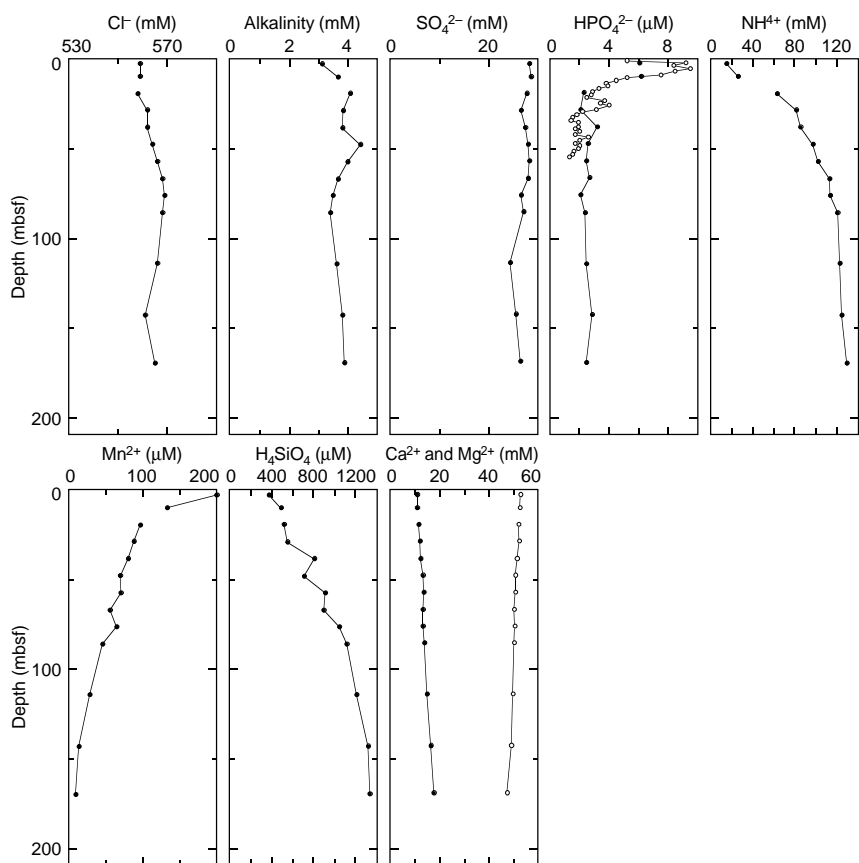


Figure 18. Interstitial water geochemical data, Site 1010. Uppermost two data points in each profile are from Hole 1010B, the others are from Hole 1010C. Solid circles = Ca, open circles = Mg.

Table 17. Concentrations of methane (C₁), ethane/ethene (C₂), and propane/propene (C₃) obtained by the headspace technique.

Core, section, interval (cm)	Depth (mbsf)	C ₁ (ppm)	C ₂ (ppm)	C ₃ (ppm)	C ₁ /C ₂	C ₂ /C ₃
167-1010A-1H-4, 145-150	5.98	3	0	0		
167-1010B-1H-3, 0-5	3.03	2	0	0		
2H-5, 0-5	6.03	3	0	0		
3H-5, 0-5	6.03	4	0	0		
167-1010C-3H-4, 0-5	19.53	6	0	0		
4H-4, 0-5	29.03	4	0	0		
5H-4, 0-5	38.53	4	0	0		
6H-4, 0-5	48.03	4	0	0		
7H-4, 0-5	57.53	5	0	0		
8H-4, 0-5	67.03	5	0	0		
9H-4, 0-5	76.53	4	0	0		
10H-4, 0-5	86.03	4	0	0		
11H-4, 0-5	95.53	3	0	0		
12H-4, 0-5	105.03	3	0	0		
13H-4, 0-5	114.53	3	0	0		
14H-4, 0-5	124.03	2	0	0		
15H-4, 0-5	133.53	2	0	0		
16H-4, 0-5	143.03	3	0	0		
17H-4, 0-5	152.53	3	0	0		
18X-4, 0-5	162.03	3	0	0		
19X-4, 0-5	169.73	3	0	0		
20X-3, 0-5	177.90	2	0	0		
21X-1, 81-86	185.44	2	0	0		
22X-1, 95-100	195.18	518	378	167	1.37	3.10
23X-1, 59-60	204.40	25	14	6	1.79	4.17
23X-CC, 30-32	207.40	99	66	29	1.50	3.41

Table 18. Concentrations of total carbon, inorganic carbon, total organic carbon, calcium carbonate, total nitrogen, and total sulfur in weight percent (wt%) from sediments of Hole 1010B.

Core, section, interval (cm)	Depth (mbsf)	Total carbon (wt%)	Inorganic carbon (wt%)	Total organic carbon (wt%)	CaCO ₃ (wt%)	Total nitrogen (wt%)	Total sulfur (wt%)
167-1010B-							
1H-1, 37-38	0.37	0.51	0.10	0.41	0.83	0.08	0.13
1H-2, 37-38	1.87	0.56	0.29	0.27	2.42	0.06	0.03
1H-3, 37-38	3.37	0.55	0.12	0.43	1.00	0.08	0.03
2H-1, 41-43	4.61	0.41	0.13	0.28	1.08	0.07	0.00
2H-2, 38-40	6.08	0.45	0.72	0.00	6.00	0.07	0.00
2H-3, 38-40	7.58	0.40	0.14	0.26	1.17	0.06	0.00
2H-4, 38-40	9.08	0.46	0.13	0.33	1.08	0.07	0.00
2H-5, 38-40	10.58	0.40	0.23	0.17	1.92	0.05	0.00
2H-6, 38-40	12.08	2.46	2.04	0.42	16.99	0.06	0.00
2H-7, 38-40	13.58	0.49	0.12	0.37	1.00	0.07	0.00

Only a part of this table is reproduced here . The entire table is on CD-ROM, back pocket, this volume.

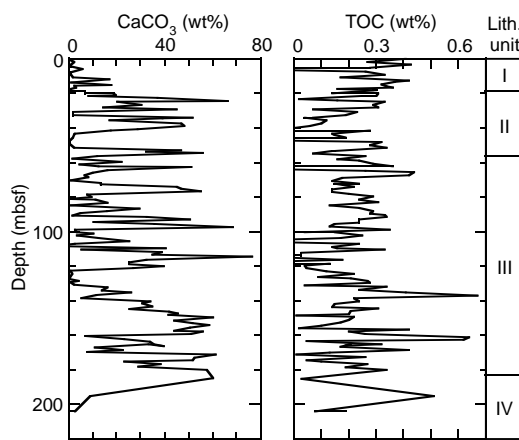


Figure 19. Calcium carbonate and total organic carbon data in weight percent (wt%) vs. depth (mbsf) from sediments of Hole 1010B. Right column indicates lithostratigraphic units as defined in the “Lithostratigraphy” section, this chapter.

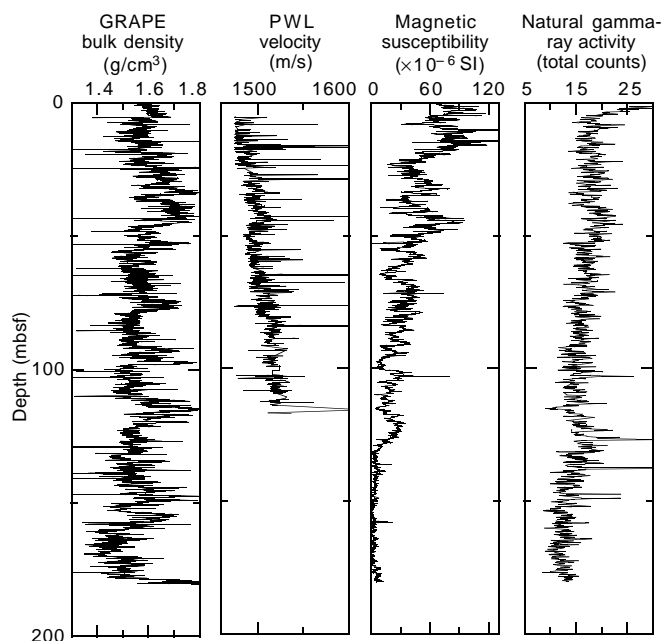


Figure 20. MST data from Hole 1010C.

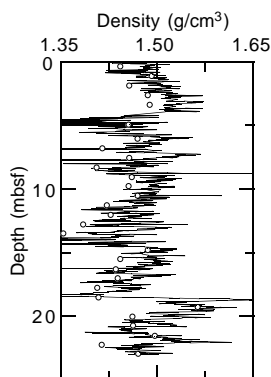


Figure 21. GRAPE bulk density (line) and discrete bulk density (circles) data from Hole 1010B.

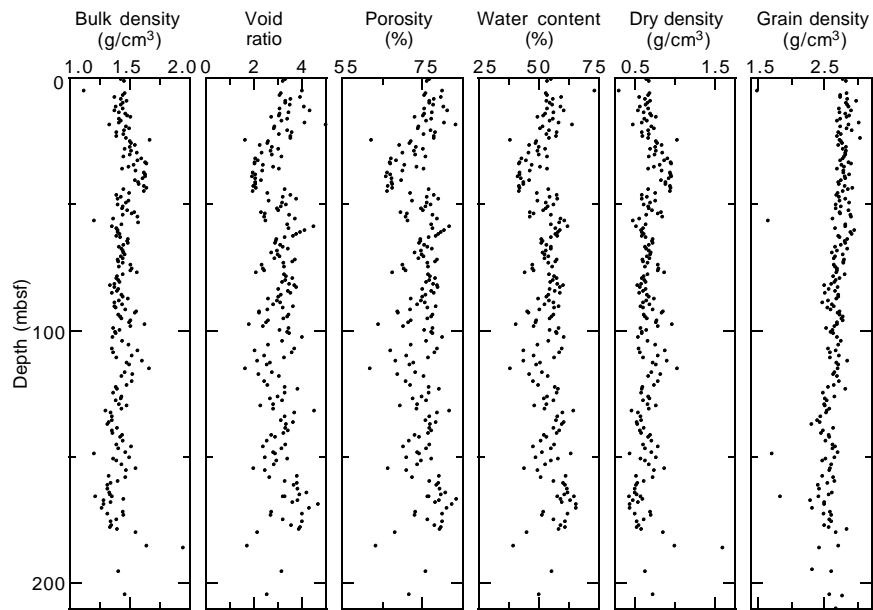


Figure 22. Index property data from Hole 1010C.

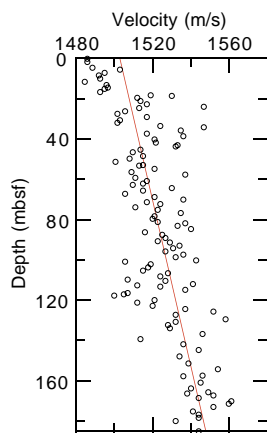


Figure 23. Discrete velocity values from Hole 1010C showing an increase downhole.

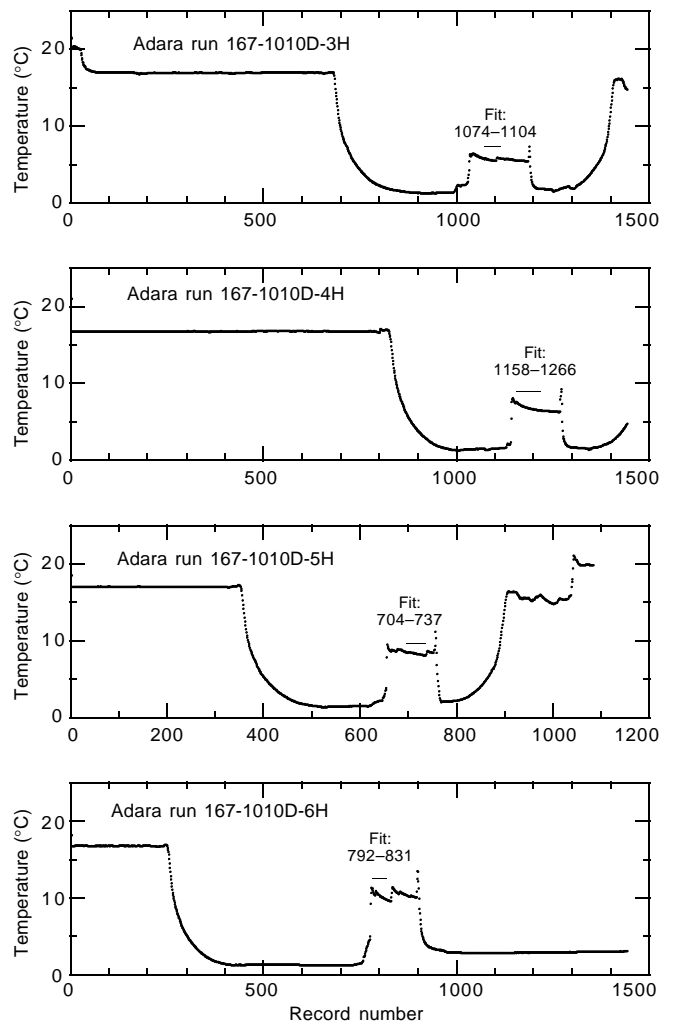


Figure 24. Hole 1010D downhole temperature vs. record number (5-s recording frequency) for each measurement run, showing the interval fitted to determine the downhole temperature.

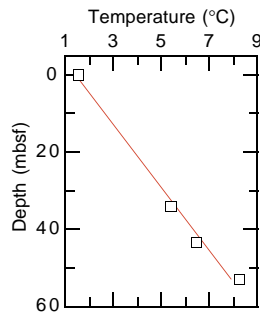


Figure 25. Downhole temperature gradient for Hole 1010C.

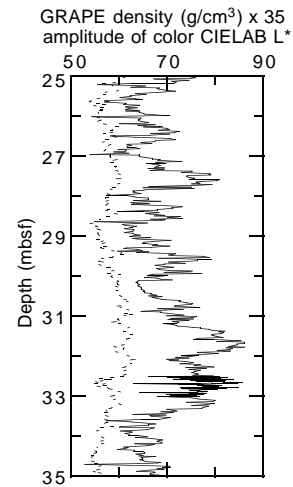


Figure 27. Intensity of color CIELAB L* from the digital color video (unitless ratio with a range from 0 to 100, shown as a line) and GRAPE bulk density (values in g/cm^3 times a factor of 35 shown as a dashed line) for Hole 1010D. The CIELAB L* data is decimated to a 2-cm interval.

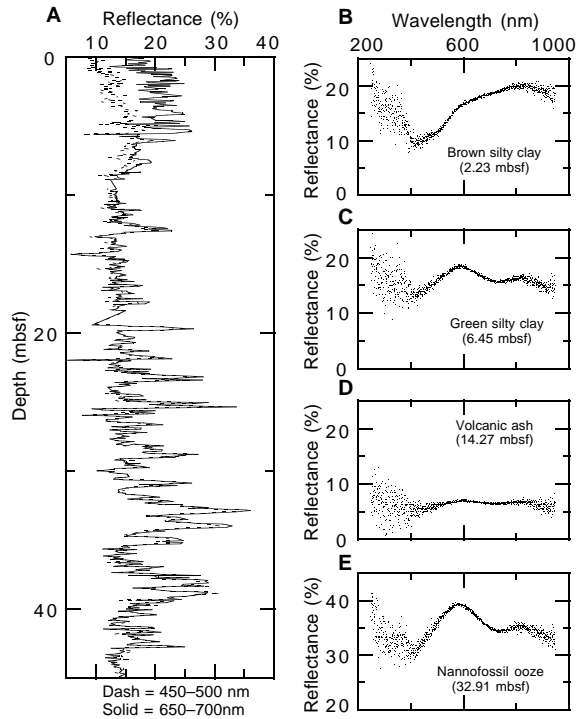


Figure 26. Summary of color reflectance data at Site 1010. **A.** Percent reflectance of two band averages (450–500 and 650–700 nm) for the upper 50 m in Hole 1010E. **B.** Characteristic spectra of silty clay above the brown/green transition. **C.** Characteristic spectra of silty clay below the transition. **D.** Low-reflectance, flat-spectrum ash layer. **E.** High-reflectance spectra characteristic of nannofossil ooze.

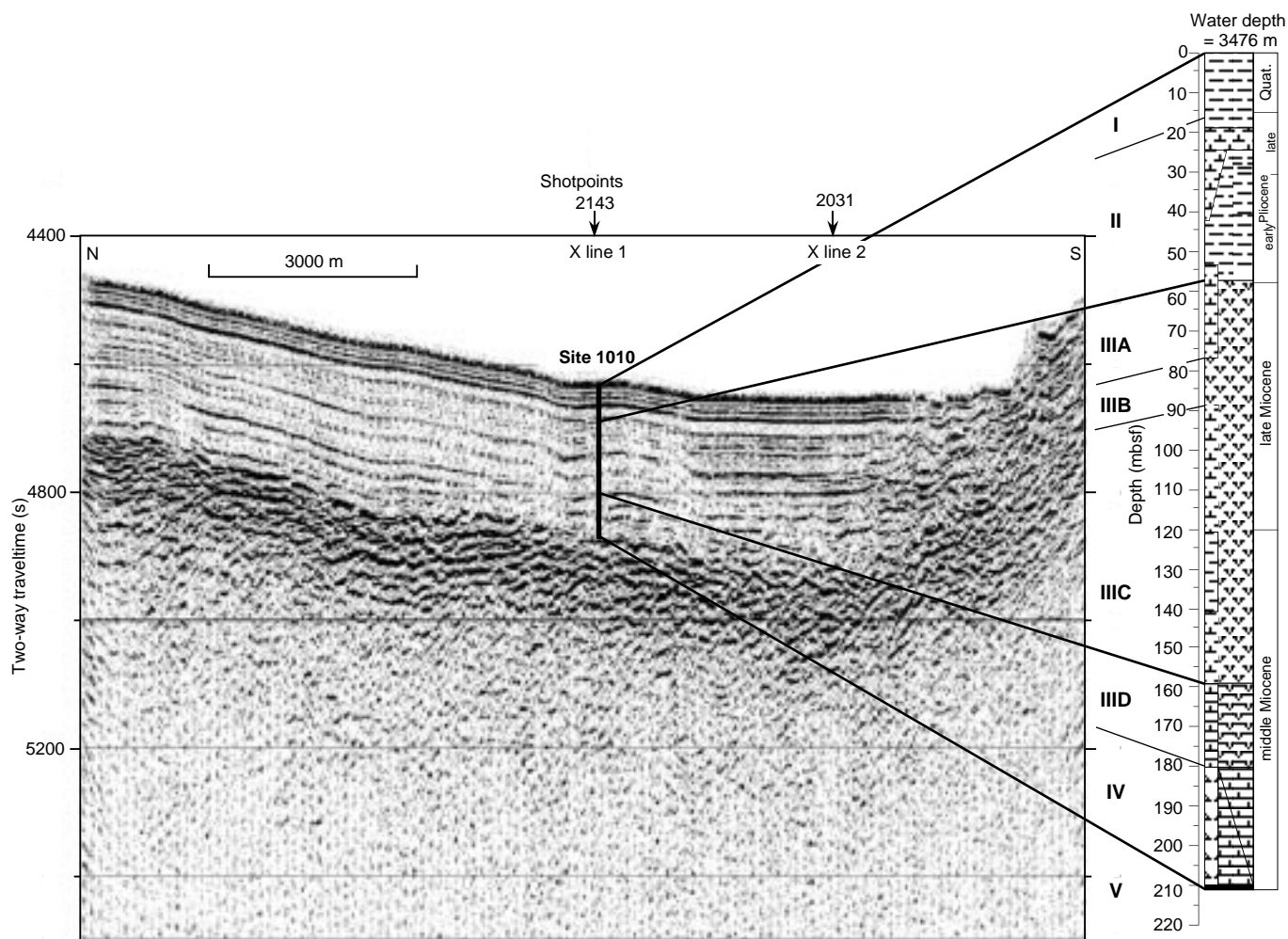


Figure 28. Comparison of the lithostratigraphic column at Site 1010 to the seismic reflection profile through the site (Lyle et al., 1995a, 1995b). Ties between the sediment column and seismic profile are estimated from the depth to basement and measured seismic velocities (see “Physical Properties” section, this chapter). On y-axis, (s) = milliseconds.